

Mixed Higgsino Dark Matter from a Reduced $SU(3)$ Gaugino Mass: Consequences for Dark Matter and Collider Searches

**Howard Baer^a, Azar Mustafayev^a, Eun-Kyung Park^a, Stefano Profumo^b and
 Xerxes Tata^c**

^a*Department of Physics, Florida State University Tallahassee, FL 32306, USA*

^b*Division of Physics, Mathematics and Astronomy, California Institute of Technology,
 Mail Code 106-38, Pasadena, CA 91125, USA*

^c*Department of Physics and Astronomy, University of Hawaii, Honolulu, HI 96822, USA*

E-mail: baer@hep.fsu.edu, mazar@hep.fsu.edu, epark@hep.fsu.edu,
 profumo@caltech.edu, tata@phys.hawaii.edu

ABSTRACT: In gravity-mediated SUSY breaking models with non-universal gaugino masses, lowering the $SU(3)$ gaugino mass $|M_3|$ leads to a reduction in the squark and gluino masses. Lower third generation squark masses, in turn, diminish the effect of a large top quark Yukawa coupling in the running of the higgs mass parameter $m_{H_u}^2$, leading to a reduction in the magnitude of the superpotential μ parameter (relative to M_1 and M_2). A low $|\mu|$ parameter gives rise to mixed higgsino dark matter (MHDM), which can efficiently annihilate in the early universe to give a dark matter relic density in accord with WMAP measurements. We explore the phenomenology of the low $|M_3|$ scenario, and find for the case of MHDM increased rates for direct and indirect detection of neutralino dark matter relative to the mSUGRA model. The sparticle mass spectrum is characterized by relatively light gluinos, frequently with $m_{\tilde{g}} \ll m_{\tilde{q}}$. If scalar masses are large, then gluinos can be very light, with $\tilde{g} \rightarrow \tilde{Z}_1 g$ loop decays dominating the gluino branching fraction. Top squarks can be much lighter than sbottom and first/second generation squarks. The presence of low mass higgsino-like charginos and neutralinos is expected at the CERN LHC. The small $m_{\tilde{Z}_2} - m_{\tilde{Z}_1}$ mass gap should give rise to a visible opposite-sign/same flavor dilepton mass edge. At a TeV scale linear e^+e^- collider, the region of MHDM will mean that the entire spectrum of charginos and neutralinos are amongst the lightest sparticles, and are most likely to be produced at observable rates, allowing for a complete reconstruction of the gaugino-higgsino sector.

KEYWORDS: Supersymmetry Phenomenology, Supersymmetric Standard Model, Dark Matter.

1. Introduction

Recently, a variety of astrophysical measurements by the WMAP[1] and other collaborations have determined the density of cold dark matter (CDM) in the universe to be

$$\Omega_{CDM}h^2 = 0.113 \pm 0.009. \quad (1.1)$$

The additional determination of a non-zero dark energy component to the universe suggests that we live in a Λ CDM universe, with $\Omega_{\Lambda}h^2 \sim 0.35$. While the nature of dark energy remains a mystery, there are a number of well-motivated particle physics candidates for the CDM, and collider and DM search experiments may serve to distinguish between the various possibilities in the near future.

One of the especially intriguing features of R -parity conserving supersymmetric models is that they provide a natural candidate for cold dark matter (CDM) in the universe[2, 3]. The lightest neutralino \tilde{Z}_1 in gravity-mediated SUSY breaking models (SUGRA) is especially appealing as a DM candidate in that it can be produced thermally in the early universe, and the calculable relic abundance turns out to be in the right neighborhood to match the measurements of the density of CDM in the universe.

Many analyses of neutralino CDM have been performed[4] within the context of the paradigm minimal supergravity model[5] (mSUGRA), which is completely specified by the parameter set

$$m_0, m_{1/2}, A_0, \tan \beta \text{ and } sign(\mu). \quad (1.2)$$

The mSUGRA model assumes that the minimal supersymmetric Standard Model (MSSM) is valid between the mass scales $Q = M_{GUT}$ and $Q = M_{\text{weak}}$. A common value m_0 ($m_{1/2}$) ((A_0)) is assumed for all scalar mass (gaugino mass) ((trilinear soft SUSY breaking)) parameters at $Q = M_{GUT}$, and $\tan \beta$ is the ratio of vacuum expectation values of the two Higgs fields that give masses to the up and down type fermions. The magnitude of the superpotential Higgs mass term μ , but not its sign, is fixed so as to reproduce the observed Z boson mass. The values of couplings and other model parameters renormalized at the weak scale can be computed via renormalization group (RG) evolution from $Q = M_{GUT}$ to $Q = M_{\text{weak}}$. From these weak scale parameters, sparticle masses and mixings may be computed, and the associated relic density of neutralinos as well as scattering cross sections and decay rates can be determined.

In most of the allowed mSUGRA parameter space, the relic density $\Omega_{\tilde{Z}_1}h^2$ turns out to be considerably larger than the WMAP value. Consistency with WMAP thus implies that neutralinos should be able to annihilate very efficiently in the early universe. In the mSUGRA model, the annihilation rate is enhanced in just the following regions of parameter space, where the sparticle masses and/or the neutralino composition assume special forms.

- The bulk region occurs at low values of m_0 and $m_{1/2}$ [2, 6]. In this region, neutralino annihilation is enhanced by t -channel exchange of relatively light sleptons. The bulk region, featured prominently in many early analyses of the relic density, has been squeezed from below by the LEP2 bound on the chargino mass $m_{\widetilde{W}_1} > 103.5$ GeV

and the measured value of the branching fraction $B(b \rightarrow s\gamma)$, and from above by the tight bound from WMAP.

- The stau co-annihilation region occurs at low m_0 for almost any $m_{1/2}$ value where $m_{\tilde{\tau}_1} \simeq m_{\tilde{Z}_1}$. The staus, being charged, can annihilate rapidly so that $\tilde{\tau}_1 \tilde{Z}_1$ co-annihilation processes that maintain \tilde{Z}_1 in thermal equilibrium with $\tilde{\tau}_1$, serve to reduce the relic density of neutralinos [7].
- The hyperbolic branch/focus point (HB/FP) region at large $m_0 \sim$ several TeV, where $|\mu|$ becomes small, and neutralinos efficiently annihilate via their higgsino components[8]. This is the case of mixed higgsino dark matter (MHDM).
- The A -annihilation funnel occurs at large $\tan \beta$ values when $2m_{\tilde{Z}_1} \sim m_A$ (or m_H) and neutralinos can efficiently annihilate through the relatively broad A and H Higgs resonances[9].

In addition, a less prominent light Higgs h annihilation corridor occurs at low $m_{1/2}$ [10] and a top squark co-annihilation region occurs at particular A_0 values when $m_{\tilde{t}_1} \simeq m_{\tilde{Z}_1}$ [11].

Many analyses have also been performed for gravity-mediated SUSY breaking models with non-universal soft SUSY breaking (SSB) terms. Non-universality of SSB scalar masses can, 1. pull one or more scalar masses to low values so that “bulk” annihilation via t -channel exchange of light scalars can occur[12, 13], 2. bring in new near degeneracies of various sparticles with the \tilde{Z}_1 so that new co-annihilation regions open up[14, 13, 15], 3. bring the value of m_A into accord with $2m_{\tilde{Z}_1}$ so that Higgs resonance annihilation can occur[16, 13], or 4. pull the value of $|\mu|$ down so that higgsino annihilation can occur[16, 17, 13].

If non-universal gaugino masses are allowed, then qualitatively new possibilities arise that are not realized in the mSUGRA model[18, 19, 20, 21]. One case, that of mixed wino dark matter (MWDM), has been addressed in a previous paper[22]. In this case, as the weak scale value of $SU(2)$ gaugino mass $M_2(\text{weak})$ is lowered from its mSUGRA value, keeping the hypercharge gaugino mass $M_1(\text{weak})$ fixed, the wino component of \tilde{Z}_1 continuously increases until it becomes dominant when $M_2(\text{weak}) < M_1(\text{weak})$ (assuming $|\mu|$ is large). The $\tilde{Z}_1 \tilde{W}_{1,2} W$ coupling becomes large when \tilde{Z}_1 becomes wino-like, resulting in enhanced $\tilde{Z}_1 \tilde{Z}_1 \rightarrow W^+ W^-$ annihilations. Moreover, co-annihilations with the lightest chargino and with the next-to-lightest neutralino help to further suppress the thermal relic abundance of the lightest SUSY particles (LSPs). Indeed, if the wino component of the neutralino is too large, this annihilation rate is very big and the neutralino relic density falls well below the WMAP value.

A qualitatively different case arises in supersymmetric models if the SSB gaugino masses M_1 and M_2 are of opposite sign. In this case, as $|M_1|$ and $|M_2|$ approach one another, there is little bino-wino mixing, and the \tilde{Z}_1 maintains a nearly pure bino-like or wino-like identity. The WMAP relic density can nonetheless be achieved for $M_1 \simeq -M_2$ via bino-wino co-annihilation (BWCA) of the bino-like lightest neutralino. The resulting DM and collider phenomenology was investigated in Ref. [23]. The MWDM and BWCA DM scenarios were also investigated recently in Ref. [24], where these scenarios were collectively dubbed “the well-tempered neutralino”.

In this paper, we investigate a scenario where, as previously noted by Belanger *et al.*[25] and also by Nezri and Mambrini[26], a diminution of the GUT scale value of the $SU(3)$ gaugino mass M_3 relative to M_1 and M_2 leads to a sparticle spectrum with lower gluino and squark masses (the latter are lowered through RG effects due to a reduced M_3). We are motivated to consider this because by adjusting M_3 to the right value(s) provides another way to obtain MHDM. To understand this, we begin by noting that the RG equation for the soft SUSY breaking Higgs squared mass $m_{H_u}^2$ reads (in a standard notation[27])

$$\frac{dm_{H_u}^2}{dt} = \frac{2}{16\pi^2} \left(-\frac{3}{5}g_1^2 M_1^2 - 3g_2^2 M_2^2 + \frac{3}{10}g_1^2 S + 3f_t^2 X_t \right), \quad (1.3)$$

where $X_t = m_{Q_3}^2 + m_{t_R}^2 + m_{H_u}^2 + A_t^2$ and $S = m_{H_u}^2 - m_{H_d}^2 + \text{Tr}(\mathbf{m}_Q^2 - \mathbf{m}_L^2 - 2\mathbf{m}_U^2 + \mathbf{m}_D^2 + \mathbf{m}_E^2)$. Here, f_t is the top quark Yukawa coupling and $t = \log Q^2$. The $f_t^2 X_t$ term drives $m_{H_u}^2$ to negative values due to the large top quark Yukawa coupling in the celebrated radiative electroweak symmetry breaking (REWSB) mechanism[28]. In the case where $M_3 \ll M_1 \sim M_2$ at the GUT scale, the squark squared mass terms and A_t^2 (and hence X_t) are suppressed at lower scales; as a consequence, $m_{H_u}^2$ is not driven to such large negative values as in the universal gaugino mass case. Thus, if $|M_3|$ is chosen small (but not so small that $m_{H_u}^2$ is no longer driven negative), we still obtain REWSB, but with a smaller weak scale value of $-m_{H_u}^2$.¹ There is also a corresponding effect on the RG flow of $m_{H_d}^2$, but this is typically smaller because $f_b \ll f_t$ except for very large values of $\tan\beta$. The weak scale value of μ^2 (at tree-level) is then obtained from the weak scale parameters of the Higgs sector via the EWSB relation,

$$\mu^2 = \frac{m_{H_d}^2 - m_{H_u}^2 \tan^2\beta}{(\tan^2\beta - 1)} - \frac{M_Z^2}{2}. \quad (1.4)$$

We see that if $|m_{H_u}^2| \gg M_Z^2$ and moderate to large values of $\tan\beta$, $\mu^2 \sim -m_{H_u}^2$. Thus the smaller $|m_{H_u}^2|$ value expected in the low $|M_3|$ case results in a smaller $|\mu|$ parameter, and a correspondingly larger higgsino component of the lightest neutralino \tilde{Z}_1 .

This situation is illustrated in Fig. 1, where we plot the evolution of $m_{H_d}^2$, $m_{H_u}^2$, and the gaugino mass parameters versus the renormalization scale Q from $Q = M_{\text{GUT}}$ to $Q = M_{\text{weak}}$ for the mSUGRA model with $m_0 = m_{1/2} = 300$ GeV, $A_0 = 0$, $\tan\beta = 10$, $\mu > 0$ and $m_t = 175$ GeV (solid curves), and for the case of $M_3 = 0.5m_{1/2}$ (dashed curves). The electroweak gaugino mass parameters evolve identically at the one loop level, and the tiny difference seen is a two loop effect. The gluino mass parameter, on the other hand, starts off at a smaller value and evolves to a correspondingly smaller value at the weak scale. Turning to the mass parameters in the Higgs sector, we see that, as expected, $m_{H_u}^2$ runs to a less negative value in the case of the low M_3 model than in the case of the mSUGRA model with universality of the GUT scale gaugino mass parameters. The evolution of $m_{H_d}^2$ is very similar in the two cases because the bottom Yukawa coupling is very small.

This reduction of μ is illustrated as well in Fig. 2, where we show the behaviour of μ as a function of the ratio $|M_3|/m_{1/2}$, for several values of m_0 , again with $A_0 = 0$, $\tan\beta = 10$, $\mu > 0$ and $m_t = 175$ GeV. The curves end where REWSB is no longer viable because $m_{H_u}^2$

¹Indeed, for given values of other parameters, the constraint of REWSB imposes a lower bound on $|M_3|$.

$$m_0 = 300 \text{ GeV}, m_{1/2} = 300 \text{ GeV}, \tan\beta = 10, A_0 = 0, \mu > 0, m_t = 175 \text{ GeV}$$

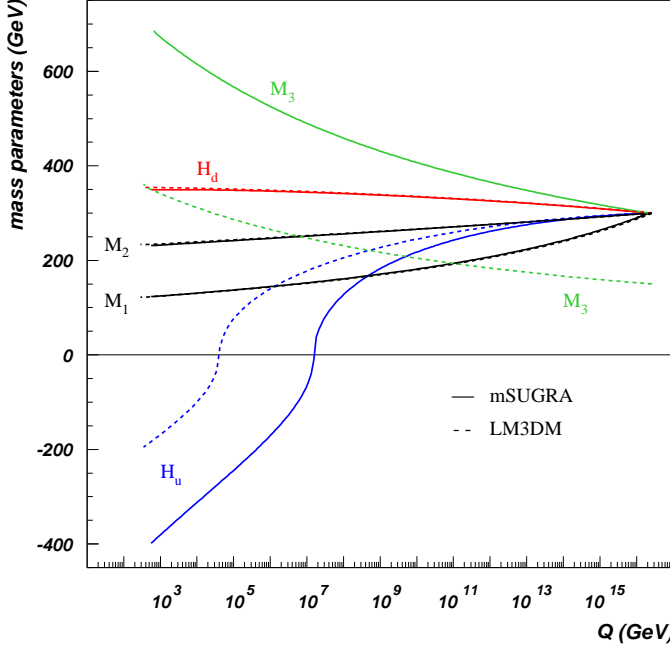


Figure 1: Evolution of the soft SUSY breaking Higgs mass parameters $\text{sign}(m_{H_u}^2) \sqrt{|m_{H_u}^2|}$ and $\text{sign}(m_{H_d}^2) \sqrt{|m_{H_d}^2|}$ as a function of scale Q in the mSUGRA model (solid) for $m_0 = 300$ GeV, $m_{1/2} = 300$ GeV, $A_0 = 0$, $\tan\beta = 10$, $\mu > 0$ and $m_t = 175$ GeV. The same running mass parameters are shown for LM3DM for the same parameters as in the mSUGRA case except taking $M_3 = 0.5m_{1/2}$ at M_{GUT} (dashes). Also shown is the corresponding evolution of gaugino mass parameters M_1 , M_2 and M_3 , for the mSUGRA case (solid) and the $M_3 = 0.5m_{1/2}$ case (dashes).

does not evolve to negative values. We see that for relatively low values of m_0 (smaller than a few times $m_{1/2}$), low values of μ are achieved for $|M_3|/m_{1/2} < 1$, while for very large values of m_0 (that, for the chosen value of $m_{1/2}$ may have been forbidden for the mSUGRA case), REWSB with low values of $|\mu|$ becomes possible but only for $|M_3|/m_{1/2} > 1$. These low $|\mu|$ regions are just generalizations of the well-known HB/FB regions of the mSUGRA model. The location of the “generalized” HP/FB region in the $m_0 - m_{1/2}$ plane of the extended model depends on the value of $r_3 \equiv M_3/m_{1/2}$: it lies to the left (right) of the corresponding region in the mSUGRA model if $|r_3| < 1$ ($|r_3| > 1$). In the study presented here we focus on the first possibility, as it leads to lighter coloured sparticles that may well be accessible at the CERN Large Hadron Collider (LHC) scheduled to commence operations next year. At the same time, the large higgsino component expected in this low M_3 dark matter (LM3DM) scenario should lead to larger detection rates relative to mSUGRA in direct and indirect searches for neutralino dark matter.

Many previous studies have examined the neutralino relic density in models with gaugino mass non-universality, along with prospects for direct and indirect detection of DM neutralinos. Griest and Roszkowski[29] first pointed out that a wide range of relic density

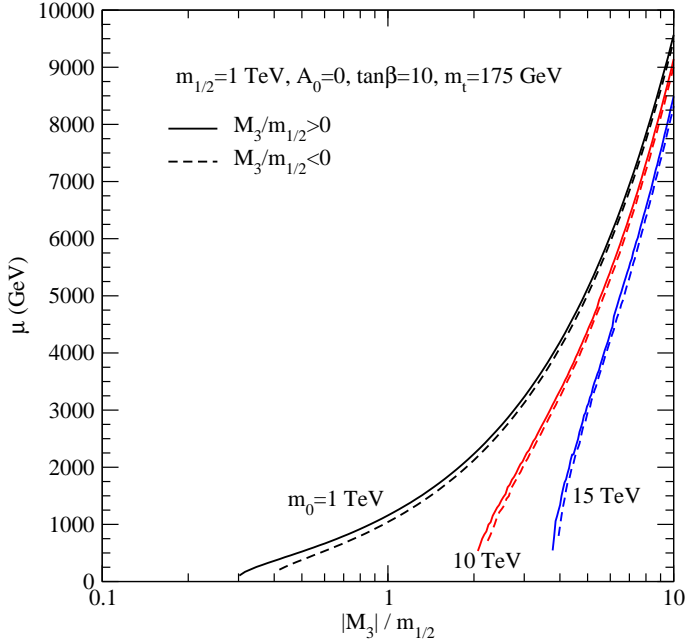


Figure 2: The values of μ dictated by REWSB as a function of $|M_3|/m_{1/2}$, for $A_0 = 0$, $\tan \beta = 10$, $\mu > 0$ and $m_t = 175$ GeV, at various values of m_0

values could be obtained by abandoning gaugino mass universality by allowing departures from $M_1/M_2 \simeq 0.5$. Anomaly-mediated SUSY breaking models, where the gaugino masses are proportional to the β -functions of the corresponding low energy gauge groups have $M_1 : M_2 : M_3 \sim 3 : 1 : -10$. As a result, the \tilde{Z}_1 is almost a pure wino which annihilates very efficiently, resulting in too low a thermal relic neutralino density: to account for the observed dark matter density, Moroi and Randall[30] invoked the decay of heavy moduli to wino-like neutralinos in the early history of the universe. The dark matter relic density and detection rates in models with non-minimal $SU(5)$ gauge kinetic function, and also in O-II string models were studied by Corsetti and Nath[31]. Birkedal-Hanson and Nelson showed that a GUT scale ratio $M_1/M_2 \sim 1.5$ would bring the relic density into accord with the measured CDM density via MWDM, and also presented direct detection rates[32]. Bertin, Nezri and Orloff studied the variation of relic density and the enhancements in direct and indirect DM detection rates as gaugino mass ratios are varied[33]. Bottino *et al.* performed scans over independent weak scale parameters to show variation in indirect DM detection rates, and noted that neutralinos as low as 6 GeV are allowed[34]. Mambrini and Muñoz, and also Cerdene and Muñoz, examined direct and indirect detection rates for models with non-universal scalar and gaugino masses[35]. Auto *et al.*[14] proposed non-universal gaugino masses to reconcile the predicted relic density in models with Yukawa coupling unification with the WMAP result. Masiero, Profumo and Ullio exhibit the relic density and direct and indirect detection rates in split supersymmetry where M_1 , M_2 and μ are taken as independent weak scale parameters with ultra-heavy squarks and sleptons[36]. Finally, as mentioned above, the variation of the relic density due to the change of M_3 – the subject of this paper – was first studied by Belanger *et al.* who showed that large swaths

of the $m_0 - m_{1/2}$ plane are consistent with the WMAP value when the $SU(3)$ gaugino mass M_3 becomes small [25]; this topic was subsequently also studied by Mambrini and Nezri[26].

It has been shown that the various non-universal scenarios each lead to distinctive phenomenologies, and can be distinguished from mSUGRA and from one another via their implications for accelerator experiments, and simultaneously, for direct and indirect searches for DM. The purpose of this paper is to study WMAP viable SUSY models with a non-universal GUT scale gaugino mass hierarchy $|M_3| \ll M_1 \simeq M_2$ – these models have received relatively little attention in the literature – and to explore their phenomenology. In regions of parameter space that yield the observed relic density of MHDM, we examine prospects for its direct and indirect detection, and also outline the impact on prospects for direct detection of sparticles at the Fermilab Tevatron, the CERN LHC and at the future international linear e^+e^- collider (ILC). For expediency, we adopt an mSUGRA-like model with universal GUT scale SSB parameters, but with the $SU(3)$ gaugino mass as one additional parameter; *i.e.* we take $M_1 = M_2 \equiv m_{1/2} > 0$ at $Q = M_{GUT}$, while allowing $M_3(M_{GUT})$ to remain as a free parameter with either sign. By dialing $|M_3|$ to low enough values (for the range of m_0 that we consider) any point in the remainder of the parameter space can be WMAP allowed. The parameter space naturally divides into regions with bino dark matter (BDM), or with MHDM. Once the WMAP constraint is fulfilled, then in the MHDM case one finds generally enhanced rates for direct and indirect DM detection. As far as colliders go, a mass spectrum with $m_{\tilde{q}} \simeq m_{\tilde{\ell}}$ is predicted in the scalar sector. In the gaugino sector, a much reduced mass gap of $m_{\tilde{g}} - m_{\widetilde{W}_1}$ is expected as compared to mSUGRA. This means in part that lighter gluinos can be allowed despite the constraints from LEP2, and that the Fermilab Tevatron may explore a substantial portion of the LM3DM parameter space via gluino pair production. We find that in the portion of the parameter space where $m_{\tilde{g}}/M_2$ is most suppressed, m_0 is necessarily large, and the radiative decays $\tilde{g} \rightarrow g\tilde{Z}_i$ constitute the dominant decay modes of the gluino. In this case, gluino pair production may lead to dijet + E_T^{miss} events at hadron colliders. At the CERN LHC, an enhanced reach is found in m_0 *vs.* $m_{1/2}$ parameter space relative to the mSUGRA model due to the reduced squark and gluino masses. At a linear e^+e^- collider, a much lighter spectrum of squarks and gluinos is expected. In the case of MHDM, the low μ parameter implies that the entire spectrum of charginos and neutralinos is rather light, and may be accessible to ILC searches for new sparticles.

The remainder of this paper is organized as follows. In Sec. 2, we outline the parameter space of the LM3DM scenario, and show that any point in parameter space may be WMAP allowed if a suitably low value of $|M_3|$ is adopted. We also illustrate characteristic features of the sparticle mass spectrum expected in this scenario. In Sec. 3, we discuss expectations for direct and indirect detection of neutralino DM in the LM3DM scenario, and show that generally enhanced detection rates are expected if MHDM occurs. In Sec. 4, we give an overview of some of the main features of the LM3DM scenario which give rise to distinct signatures at the Fermilab Tevatron, the CERN LHC and a $\sqrt{s} = 0.5 - 1$ TeV ILC. In Sec. 5, we present a summary of our results and some conclusions.

Note added: As this paper was being finalized, the WMAP collaboration released their

three year data along with implications for cosmology[37]. Their new central value of $\Omega_{\text{CDM}}h^2$ (and of course, the quoted error) is slightly lower than in (1.1). However, the central value obtained by combining the WMAP data with other data as in Table 6 of Ref. [37] is almost unchanged from (1.1). In either case, our analysis is hardly affected.

2. Parameter space and mass spectrum in the LM3DM scenario

As discussed in the previous section, the LM3DM scenario is completely specified by the parameter set:

$$m_0, m_{1/2}, M_3, A_0, \tan \beta, \text{ and } \text{sign}(\mu), \quad (2.1)$$

(together with m_t which we fix to be 175 GeV), where we assume $M_1 = M_2 \equiv m_{1/2} \geq 0$ at $Q = M_{\text{GUT}}$, and where M_3 can assume either sign. The assumed equality of M_1 and M_2 can be relaxed somewhat and our conclusions suffer little qualitative change so long as $M_1 \simeq M_2$. To calculate the sparticle mass spectrum, we adopt Isajet 7.73[38], which allows for the input of non-universal scalar and gaugino masses in gravity mediated SUSY breaking models where electroweak symmetry is broken radiatively. The relic density is evaluated via the IsaReD program[39], which is part of the Isatools package. IsaReD evaluates all $2 \rightarrow 2$ tree level neutralino annihilation and co-annihilation processes and implements relativistic thermal averaging in the relic density calculation.

We begin our discussion with an illustration to show that any point in mSUGRA model parameter space that is WMAP disallowed owing to too large a relic density $\Omega_{\tilde{Z}_1}h^2$, can become WMAP allowed by adjusting $|M_3|$ until a suitably small $|\mu|$ value that yields a relic density in accord with WMAP is attained. Assuming that $m_0/m_{1/2}$ is not too large, this is achieved by *lowering* $|M_3|$ from its mSUGRA value. As an example, we plot in Fig. 3a the neutralino relic density $\Omega_{\tilde{Z}_1}h^2$ vs. M_3 for $m_0 = m_{1/2} = 300$ GeV, while $A_0 = 0$, $\tan \beta = 10$ and $\mu > 0$. The value $M_3 = 300$ GeV puts us in the mSUGRA model, and here we see $\Omega_{\tilde{Z}_1}h^2 = 1.1$, and so the parameter space point would be excluded. As M_3 is lowered from its mSUGRA value, gluino and squark masses also decrease, resulting in a lower weak scale value of $|m_{H_u}^2|$ and hence $|\mu|$ as discussed in Sec. 1. At $M_3 = 150$ GeV, the value of $|\mu|$ has diminished sufficiently that the \tilde{Z}_1 is no longer bino-like, but is instead a mixed higgsino-bino state. This is illustrated in frame b), where we plot $R_{\tilde{H}} = \sqrt{v_1^{(1)2} + v_2^{(1)2}}$ (in the notation of Ref. [27]), which gives an indication of the higgsino components of the \tilde{Z}_1 . As M_3 is decreased even further, the relic density reaches a minimum around $M_3 \sim 110$ GeV, and then increases slightly before reaching the LEP2 limit where $m_{\tilde{W}_1}$ becomes less than 103.5 GeV. This slight increase occurs because $m_{\tilde{Z}_1}$ drops below M_Z and then M_W , so that $\tilde{Z}_1\tilde{Z}_1 \rightarrow ZZ, W^+W^-$ processes, the major LSP annihilation modes in the early universe become kinematically suppressed. Since there is no reason to favour the positive sign of M_3 , we show the behavior of the relic density and $R_{\tilde{H}}$ for negative M_3 as well, and note that these are nearly symmetrical under $M_3 \rightarrow -M_3$.

The effect on the sparticle mass spectrum of lowering the magnitude of the $SU(3)$ gaugino mass M_3 is shown in Fig. 4, where we plot the sparticle mass spectrum versus the ratio $r_3 = M_3/m_{1/2}$ for the same parameters as in Fig. 3. At $r_3 = 1$, we see the usual

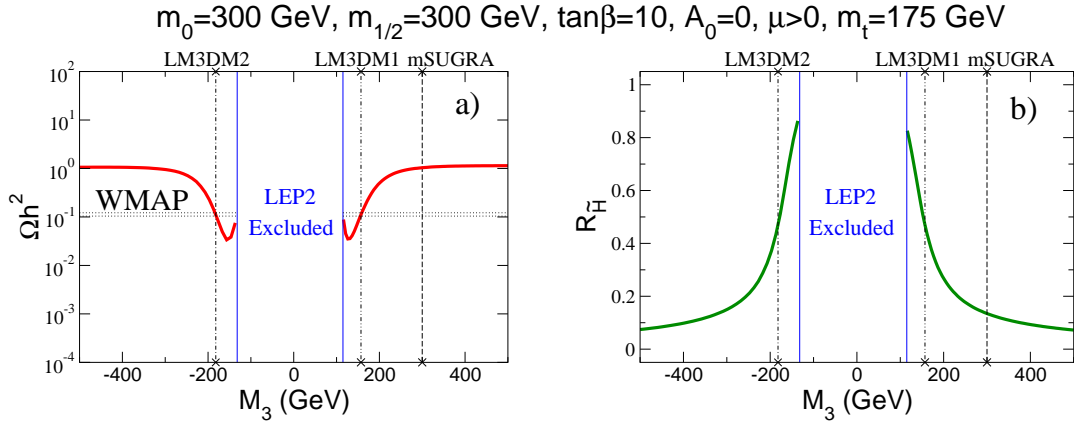


Figure 3: *a)* The neutralino relic density $\Omega_{CDM} h^2$, and *b)* higgsino component $R_{\tilde{H}}$ of the lightest neutralino as a function of M_3 for $m_0 = 300$ GeV, $m_{1/2} = 300$ GeV, $A_0 = 0$, $\tan \beta = 10$, $\mu > 0$ and $m_t = 175$ GeV.

hierarchy of sparticle masses as obtained in the mSUGRA model. As M_3 is lowered, the gluino masses reduces sharply from $m_{\tilde{g}} = 727$ GeV in the mSUGRA case to $m_{\tilde{g}} \simeq 400$ GeV for $r_3 = 0.5$ where $\Omega_{\tilde{Z}_1} h^2 = 0.11$. The reduction of M_3 reduces the renormalization suffered by the squark mass parameters, and causes the squark masses to correspondingly drop from the vicinity of 700 GeV in mSUGRA to ~ 500 GeV for $r_3 = 0.5$. On the other hand, slepton mass parameters, whose renormalization does not depend on SUSY QCD effects at the one loop level, are hardly affected by the change of M_3 . Thus, in the LM3DM scenario, the mass scale of squarks and sleptons is more nearly equal, and less hierarchical, than the case of mSUGRA at low m_0 . In fact, for the case shown in Fig. 4, the top squark \tilde{t}_1 has dropped to a lower mass than the various sleptons in the case of $r_3 = 0.5$. The value of the μ parameter is shown by the black dotted curve, and we see that this drops sharply as $|M_3|$ decreases. The drop in $|\mu|$ increases the higgsino component of the lighter charginos and neutralinos and, once they cross over to becoming higgsino-like, their masses decrease with decreasing M_3 as well.

We also show in Fig. 4 the sparticle masses for negative values of r_3 . The slepton and first/second generation squark masses are nearly symmetrical about $M_3 = 0$ because the leading (one loop) contributions to their renormalization group evolution are quadratic in the gaugino masses. However, the top squark and various chargino and neutralino masses are not symmetric. For the stops, this occurs because the RG evolution of the A parameters (A_t in this case) depends linearly on the gaugino masses. The asymmetric evolution of the A -parameters also affects $m_{H_u}^2$ and $m_{H_d}^2$ the same way; as a result, $|\mu|$, and hence chargino and neutralino masses are also not symmetric under $M_3 \rightarrow -M_3$. We see, in fact, when $M_3 < 0$, the WMAP measured value of $\Omega_{CDM} h^2$ is attained at a value of $r_3 = -0.6$, in contrast to $r_3 = 0.5$ for positive values of M_3 .

LM3DM: $m_0 = 300\text{GeV}$, $m_{1/2} = 300\text{GeV}$, $\tan\beta = 10$, $A_0 = 0$, $\mu > 0$, $m_t = 175\text{GeV}$

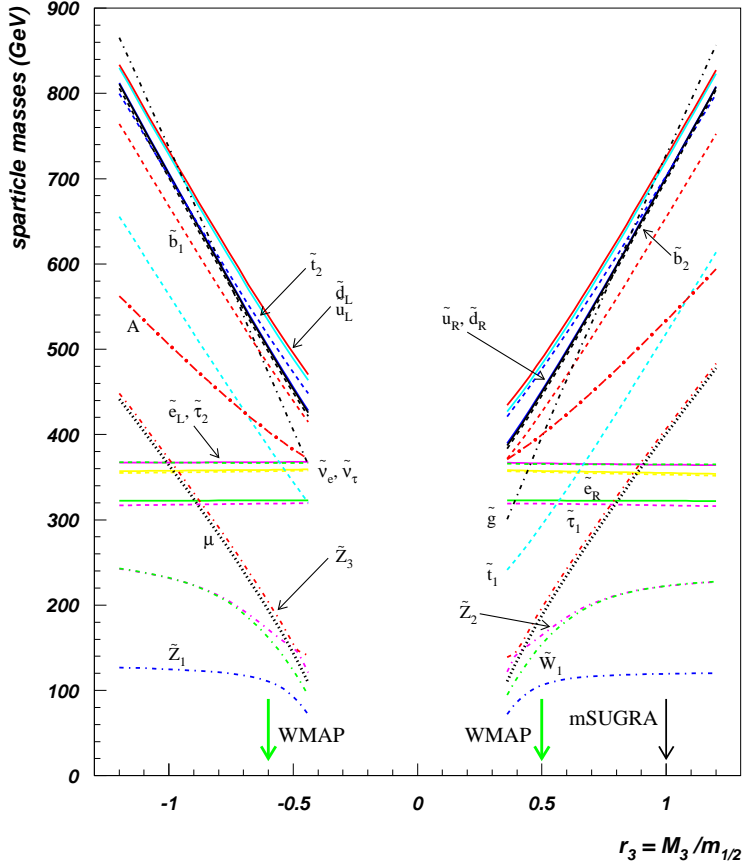


Figure 4: A plot of various sparticle and Higgs boson masses and the μ parameter *vs.* $M_3/m_{1/2}$ for $m_0 = 300$ GeV, $m_{1/2} = 300$ GeV, $A_0 = 0$, $\tan\beta = 10$ and $\mu > 0$.

Various sparticle masses are shown in Table 1 corresponding to the parameters shown in Fig. 4. We show the spectrum for the mSUGRA case, together with that for the LM3DM1 case (with $r_3 = 0.5$) and the LM3DM2 case, with $r_3 = -0.6$. In the several rows (below the masses) we show the relic density, $BF(b \rightarrow s\gamma)$, Δa_μ , and the neutralino-proton scattering cross section $\sigma(p\tilde{Z}_1)$ for these scenarios. Finally, in the last row, we show that component of the “up-type” neutral higgsino, *i.e.* that couples to the $T_3 = +1/2$ quark-squark system, in the neutralino LSP: we will return to this, as well as the LM3DM scenario in the last column of Table 1 when we discuss Tevatron signals for the gluino in the LM3DM framework.²

In Fig. 5, we show contours of r_3 in the m_0 *vs.* $m_{1/2}$ plane for $A_0 = 0$, $\tan\beta = 10$ and $\mu > 0$, where at each point in the plane $|M_3|$ has been reduced until the value of the relic

²We are aware that the value of m_h , especially in the LM3DM1 and LM3DM2 scenarios, is well below the limit from searches for the SM Higgs boson which should be applicable in these cases because m_A is large. Since the value of m_h depends on our choice of $\tan\beta$ as well of A_0 (whose precise values do not qualitatively affect the features that we discuss here), we will continue to use these scenarios as simple illustrations of the model.

parameter	mSUGRA	LM3DM1	LM3DM2	LM3DM3
m_0	300	300	300	1500
M_1	300	300	300	250
M_2	300	300	300	250
M_3	300	150	-180	50
μ	400.5	187.9	194.0	140.7
$m_{\tilde{g}}$	727.3	396.7	472.6	182.7
$m_{\tilde{u}_L}$	720.7	482.4	533.3	1492.2
$m_{\tilde{t}_1}$	518.4	293.7	385.9	838.9
$m_{\tilde{b}_1}$	654.6	426.7	482.1	1213.6
$m_{\tilde{e}_L}$	364.6	366.2	367.6	1506.2
$m_{\tilde{e}_R}$	322.3	322.6	322.7	1501.7
$m_{\tilde{W}_2}$	425.2	283.9	292.3	249.7
$m_{\tilde{W}_1}$	222.5	154.2	161.8	115.9
$m_{\tilde{Z}_4}$	426.0	286.2	294.7	254.8
$m_{\tilde{Z}_3}$	406.3	196.8	203.8	153.0
$m_{\tilde{Z}_2}$	222.3	164.9	171.4	133.1
$m_{\tilde{Z}_1}$	119.5	106.2	110.5	81.0
m_A	533.5	400.0	403.6	1496.6
m_{H^+}	542.9	410.4	414.0	1508.6
m_h	110.7	106.1	103.9	110.2
$\Omega_{\tilde{Z}_1} h^2$	1.1	0.11	0.12	0.13
$BF(b \rightarrow s\gamma)$	3.1×10^{-4}	1.6×10^{-4}	5.5×10^{-4}	3.4×10^{-4}
Δa_μ	11.9×10^{-10}	16.3×10^{-10}	15.7×10^{-10}	1.5×10^{-10}
$\sigma_{sc}(\tilde{Z}_1 p)$	1.8×10^{-9} pb	6.8×10^{-8} pb	6.7×10^{-8} pb	4.2×10^{-8} pb
$ v_1^{(1)} $	0.05	0.26	0.26	0.37

Table 1: Masses and parameters in GeV units for mSUGRA and three LM3DM scenarios. In each case, $A_0 = 0$, $\tan \beta = 10$ and $m_t = 175$ GeV.

density is found to be $\Omega_{\tilde{Z}_1} h^2 = 0.11$. Frame *a*) shows these contours for negative r_3 , while frame *b*) shows contours for $r_3 > 0$. The red shaded region on the left hand side is excluded because the $\tilde{\tau}_1$ becomes the LSP (in contradiction to search limits for stable charged or colored relics), while the blue region at low $m_{1/2}$ is excluded by the LEP2 chargino search limits, which require $m_{\tilde{W}_1} > 103.5$ GeV. Unlike in the mSUGRA model, the LEP-excluded blue region is not flat because the chargino is gaugino-like for small values of m_0 but higgsino-like as m_0 becomes large. Of course, in the stau co-annihilation region, which is tight against the boundary of the red region, the relic density is already in accord with the WMAP value even in the mSUGRA case. In the lower-left bulk region, $|M_3|$ need only be reduced to values of $r_3 \sim -0.7$ (frame *a*) or $r_3 \sim 0.6$ (frame *b*)). However, for large m_0 and low $m_{1/2}$, values of $|r_3|$ as low as ~ 0.3 are needed to reach accord with WMAP. A

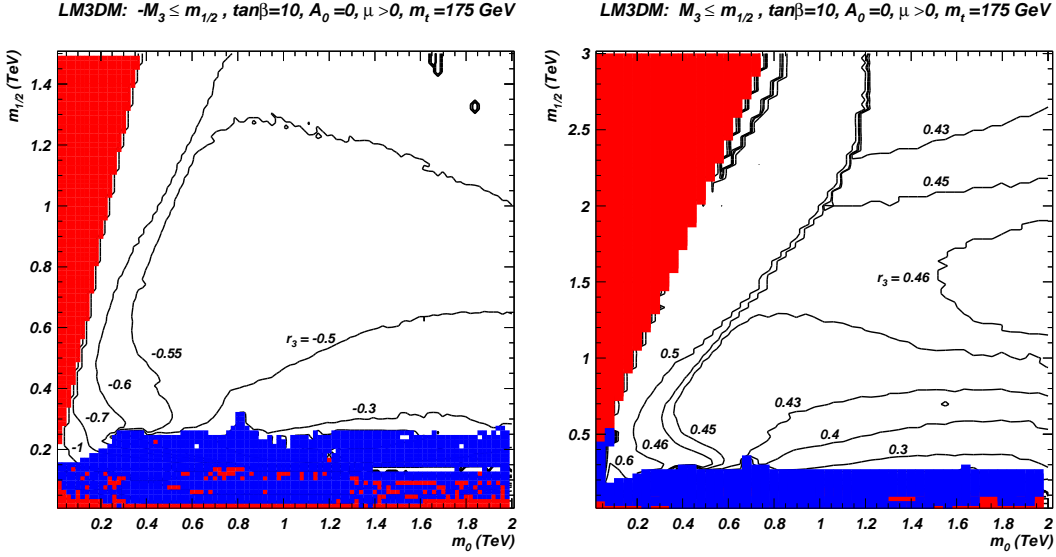


Figure 5: Contours of *a)* $r_3 < 0$ in the m_0 vs. $m_{1/2}$ plane for $m_{1/2}$ up to 1.5 TeV, with $\tan \beta = 10$, $A_0 = 0$, $\mu > 0$. Each point in the plane has r_3 dialed to such a value that $\Omega_{\tilde{Z}_1} h^2 = 0.11$. The red region on the left is excluded either because $\tilde{\tau}_1$ becomes the LSP or electroweak symmetry is not correctly broken, while the blue region is excluded by the LEP lower limit $m_{\tilde{W}_1} > 103.5$ GeV. In frame *b*), we plot contours of $r_3 > 0$ for the same parameter choices as in frame *a*), although we extend the range of $m_{1/2}$ to 3 TeV.

third case study in this region, labelled LM3DM3, is shown in the last column of Table 1.³ In most of parameter space, values of $|r_3| \sim 0.4 - 0.6$ are sufficient to match the measured relic density.

The planes of Fig. 5 naturally divide into two distinct regions. The left-hand side of each plot with $|r_3| \gtrsim 0.5 - 0.6$ is labelled the bino DM region (BDM), since here the \tilde{Z}_1 is bino-like, while the large m_0 side of the plane with $|r_3| \lesssim 0.5 - 0.6$ is labelled as MHDM, since here the \tilde{Z}_1 is mixed higgsino-bino state. The bino-wino-higgsino content of \tilde{Z}_1 for an $m_{1/2} = 1005$ GeV slice out of Fig. 5 is shown in Fig. 6.

In the BDM regions of Fig. 5, the values of M_3 and m_0 are low enough that m_A approaches $2m_{\tilde{Z}_1}$. In this case, the thermal distribution of neutralinos convoluted with the $\tilde{Z}_1 \tilde{Z}_1 \rightarrow b\bar{b}$ cross section allows for an enhanced annihilation rate via the *s*-channel *A*, *H*-pole. On the very low m_0 edge of parameter space, $\tilde{\tau}_1$ co-annihilation also contributes to a reduction in the neutralino relic density, and a wide range of r_3 is possible. As we move to larger m_0 values in Fig. 5, the value of m_A becomes much larger than $2m_{\tilde{Z}_1}$, and *A*-funnel annihilation is no longer efficient enough to reduce the relic density. Various sparticle and Higgs masses are shown as a function of m_0 in Fig. 7, for the same parameters as in Fig. 6. In this case, for large m_0 , r_3 must be reduced to lower values of $r_3 < 0.5$, and the \tilde{Z}_1 becomes MHDM. Then $\tilde{Z}_1 \tilde{Z}_1 \rightarrow WW$, ZZ , and also $\tilde{W}_1 \tilde{Z}_1$ and (to a smaller extent)

³In this case, the decays $\tilde{Z}_4 \rightarrow q\bar{q}\tilde{g}$ and the decays $\tilde{W}_2^+ \rightarrow u\bar{d}\tilde{g}$, not included in Isajet, are kinematically accessible. We expect, however, that this will not significantly affect our analysis because these sparticles will dominantly decay via their two-body modes.

$m_{1/2} = 1005 \text{ GeV}$, $M_3 \leq m_{1/2}$, $\tan\beta = 10$, $A_0 = 0$, $\mu > 0$, $m_t = 175 \text{ GeV}$

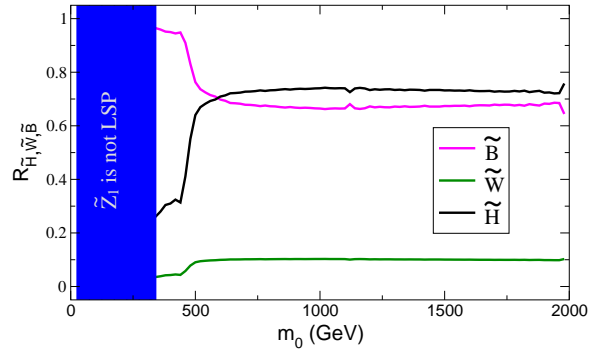


Figure 6: The bino, wino and higgsino content of the \tilde{Z}_1 versus m_0 for a $m_{1/2} = 1005 \text{ GeV}$ slice out of the plane in Fig. 5b), showing that \tilde{Z}_1 is BDM for small m_0 , and MHDM for large m_0 .

$\tilde{Z}_1 \tilde{Z}_2$ co-annihilation act to suppress the relic density. This is shown explicitly in Fig. 8, where we plot the thermally averaged neutralino annihilation cross sections integrated over temperature from freeze-out to the present time, versus m_0 for the same parameter choices as in Fig. 6. We see that the co-annihilation processes become significant only for $m_0 \gtrsim 400 \text{ GeV}$ where r_3 , and correspondingly also $|\mu|$, have become sufficiently small.

Finally, we mention that in the upper-left of frame of Fig. 5b) (which has been extended to $m_{1/2} = 3 \text{ TeV}$ to facilitate the discussion of the LHC reach in Sec. 4.2), the r_3 value drops below 0.5 near the contours at $m_0 \sim 0.8 \text{ TeV}$ and $m_{1/2} \sim 3 \text{ TeV}$. In this part of the plane, a small additional reduction in M_3 is needed to match $\Omega_{CDM} h^2 = 0.11$ because the enhancement to $\tilde{Z}_1 \tilde{Z}_1$ annihilation via amplitudes with s -channel H , A exchanges no longer obtains since $2m_{\tilde{Z}_1} > m_H, m_A$. Thus, in this upper-left region, the \tilde{Z}_1 is again MHDM.

3. Direct and indirect detection of neutralino CDM

In this section, we explore the prospects for direct and indirect detection of neutralino dark matter within the LM3DM framework [40]. We adopt the DarkSUSY code[41], interfaced to Isajet, for the computation of the various indirect detection rates, and resort to the Adiabatically Contracted N03 Halo model[42] for the dark matter distribution in the Milky Way, which tends to give higher detection rates, especially for gamma ray and anti-particle detection than other halo profiles. In this respect, our projections may be regarded as optimistic.⁴ We evaluate the following neutralino DM detection rates:

- Direct neutralino detection via underground cryogenic detectors[46]. Here, we compute the spin independent neutralino-proton scattering cross section, and compare it to expected sensitivities[47] for Stage 2 detectors (CDMS2[48], Edelweiss2[49],

⁴For a comparison of the implications of different halo model choices for indirect DM detection rates, see *e.g.* Refs. [43, 44, 45, 13].

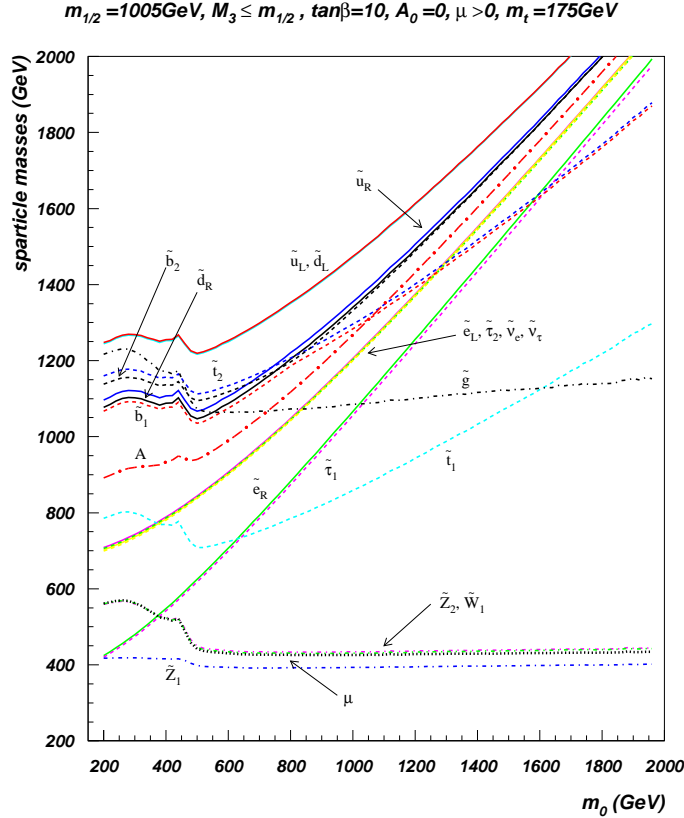


Figure 7: Sparticle masses vs. m_0 for an $m_{1/2} = 1005$ GeV slice out of the plane in Fig. 5b).

CRESST2[50], ZEPLIN2[51]) and for Stage 3, SuperCDMS, along with ton-size detectors (XENON[52], GERDA[53], ZEPLIN4[54] and WARP[55]). We adopt the projected (mass-dependent) sensitivities of CDMS2 and 1-ton XENON detectors as the experimental benchmark for direct DM detection at stage 2 and stage 3 detectors.

- Indirect detection of neutralinos via neutralino annihilation to neutrinos in the core of the Sun[56]. Here, we present rates for detection of $\nu_\mu \rightarrow \mu$ conversions at Antares[57] or IceCube[58]. The reference experimental sensitivity we use is that of IceCube, with a muon energy threshold of 50 GeV, corresponding to a flux of about 10 muons per km^2 per year.
- Indirect detection of neutralinos via neutralino annihilation in the galactic center leading to gamma rays[59], as searched for by EGRET[60], and in the future by GLAST[61]. We evaluate the integrated continuum γ ray flux above a $E_\gamma = 1$ GeV threshold, and assume a GLAST sensitivity of $1.0 \times 10^{-10} \text{ cm}^{-2}\text{s}^{-1}$.
- Indirect detection of neutralinos via neutralino annihilations in the galactic halo leading to cosmic antiparticles, including positrons[62] (HEAT[63], Pamela[64] and AMS-02[65]), antiprotons[66] (BESS[67], Pamela, AMS-02) and anti-deuterons (\bar{D}) (BESS[68], AMS-02, GAPS[69]). For positrons and antiprotons we evaluate the av-

$$m_{1/2} = 1005 \text{ GeV}, M_3 \leq m_{1/2}, \tan\beta = 10, A_0 = 0, \mu > 0, m_t = 175 \text{ GeV}$$

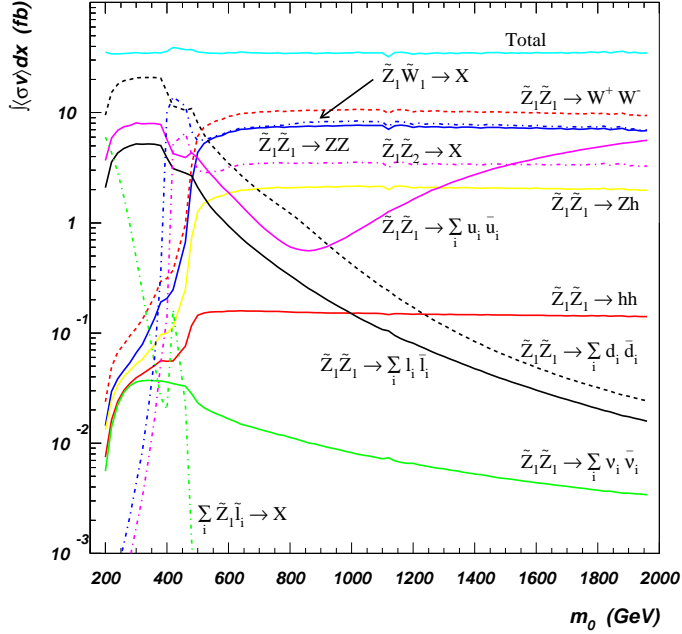


Figure 8: The thermally averaged neutralino annihilation cross sections times relative velocity integrated from $x = 0$ to x_F versus m_0 for a $m_{1/2} = 1005$ GeV slice out of the plane in Fig. 5b).

eraged differential antiparticle flux in a projected energy bin centered at a kinetic energy of 20 GeV, where we expect an optimal statistics and signal-to-background ratio at space-borne antiparticle detectors[45, 70]. We take the experimental sensitivity to be that of the Pamela experiment after three years of data-taking as our benchmark. Finally, the average differential antideuteron flux has been computed in the $0.1 < T_{\bar{D}} < 0.25$ GeV range, where $T_{\bar{D}}$ stands for the antideuteron kinetic energy per nucleon, and compared to the estimated GAPS sensitivity for an ultra-long duration balloon-borne experiment [69] (see Ref. [71] for an updated discussion of the role of antideuteron searches in DM indirect detection).

In Fig. 9, we show various direct and indirect DM detection rates for $m_0 = m_{1/2} = 300$ GeV, with $A_0 = 0$, $\tan\beta = 10$ and $\mu > 0$, while M_3 is allowed to vary. The M_3 value corresponding to the mSUGRA model is denoted by a dashed vertical line, while the LM3DM scenarios for $r_3 < 0$ and $r_3 > 0$ with $\Omega_{\tilde{Z}_1} h^2 = 0.11$ are denoted by dot-dashed and dot-dot-dashed vertical lines, respectively. The dotted lines correspond to the sensitivity level of each of these experiments; *i.e.*, the signal is observable only when the model prediction is higher than the corresponding dotted line. While the minimum sensitivity for the direct detection rates in frames *b*) – *f*) refers to the minimum magnitude of the signal that is detectable (and hence independent of the LSP mass), the smallest detectable cross section shown by the dotted curves in frame *a*) depends on the value of $m_{\tilde{Z}_1}$.

In frame *a*), we plot the spin-independent neutralino-proton scattering cross section. We see that as M_3 is decreased from its mSUGRA value, the neutralino-proton scattering

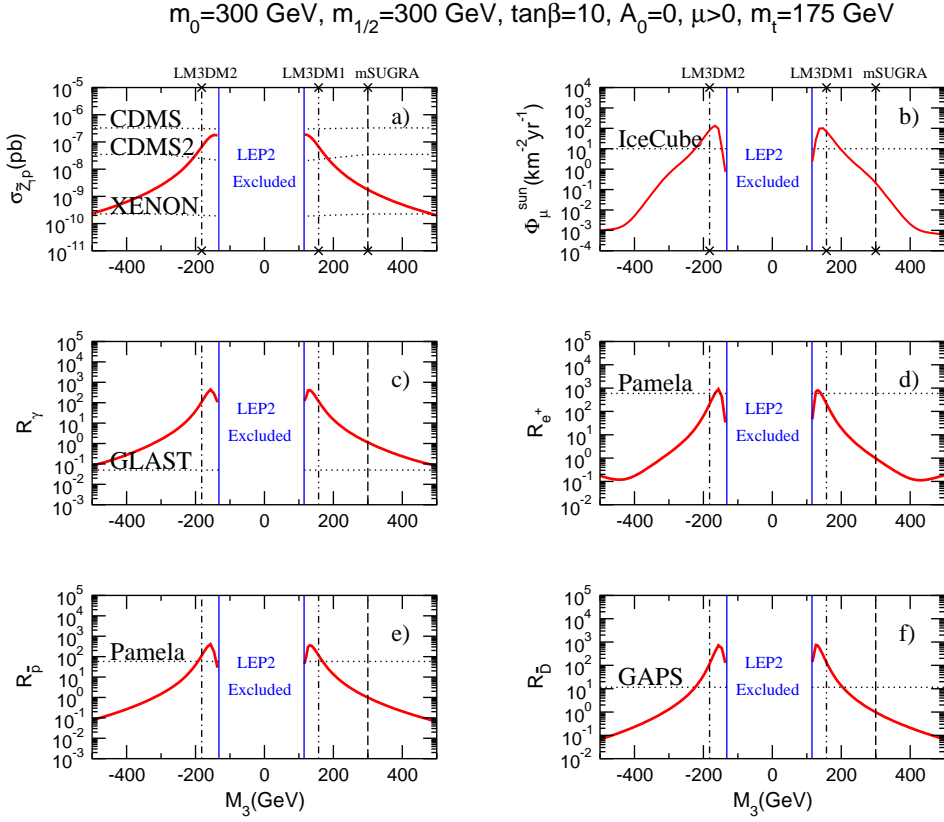


Figure 9: Rates for direct and indirect detection of neutralino dark matter vs. M_3 for $m_0 = m_{1/2} = 300 \text{ GeV}$, with $\tan\beta = 10$, $A_0 = 0$, $\mu > 0$. Frames $c)$ - $f)$ show the ratio of indirect detection rates compared to the mSUGRA model. In this figure, we adopt the adiabatically contracted N03 distribution for halo dark matter for our projections of the reach of the various experiments.

cross section rises almost two orders of magnitude to a value above $3 \times 10^{-8} \text{ pb}$, which should be detectable by CDMS2, and certainly at stage 3 detectors. A similarly large rate is attained for $r_3 < 0$, as shown in the left-hand side of frame $a)$. This frame merely reflects the well-known result that MHDM has rather large neutralino-proton scattering rates, as is typified by the HB/FP region of the mSUGRA model. The value of $\sigma_{SI}(\tilde{Z}_1p)$ is further enhanced by the lowered squark masses of the LM3DM scenario.

In frame $b)$, we show the flux of muons from neutralino pair annihilations in the core of the Sun. The expected muon flux is below the reach of IceCube in the mSUGRA framework, but increases over two orders of magnitude into the observable range for IceCube as a result of the increased higgsino content of the LSP and the reduced squark mass when the relic density is in agreement with the WMAP measurement as in the LM3DM model.

In frames $c)$, $d)$, $e)$ and $f)$ we show the flux of photons, positrons, antiprotons and antideuterons, respectively. The results here are plotted as ratios of fluxes normalized to the corresponding mSUGRA point, in order to give results that are approximately halo-

$m_{1/2} = 1005 \text{ GeV}$, $M_3 \leq m_{1/2}$, $\tan\beta = 10$, $A_0 = 0$, $\mu > 0$, $m_t = 175 \text{ GeV}$

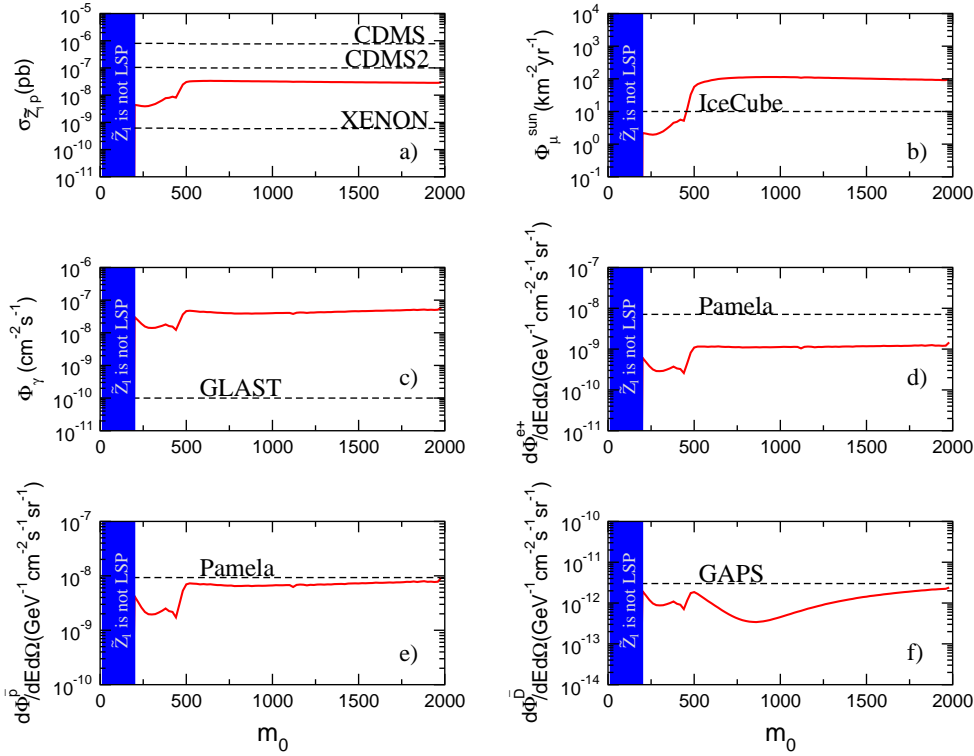


Figure 10: Rates for direct and indirect detection of neutralino dark matter vs. m_0 for the $m_{1/2} = 1005 \text{ GeV}$ slice of the plane in Fig. 5b together with the projected sensitivities of the various experiments, assuming the adiabatically contracted N03 distribution for halo dark matter.

model independent. Also shown by the horizontal lines are the expected experimental reaches, as obtained by using the Adiabatically Contracted N03 Halo model[42]. The rates for indirect detection via observation of halo annihilation remnants are typically low for bino-like DM as in the mSUGRA model. However, when $|r_3|$ is reduced until the measured CDM relic abundance is achieved, these halo annihilation signals all jump by factors of 100-200, and are much more likely to be observed by various gamma ray and antimatter detection experiments. We should, however, keep in mind that this conclusion is sensitive to our assumption of the DM halo profile.

The detectability of the same signals, but this time for the slice of the $m_{1/2} = 1005 \text{ GeV}$ slice of LM3DM parameter space we considered in Fig. 7 is illustrated in Fig. 10. The cross sections or the expected fluxes are absolutely normalized, rather than to any particular mSUGRA model. The most striking feature of this figure is the rather sudden increase (around $m_0 \sim 500 \text{ GeV}$) of the signal as m_0 increases from low values where the LSP is bino-like to high values where the required low value of r_3 leads to a significant higgsino component in the LSP.

We present an overview of the reach of direct and indirect dark matter search techniques in Fig. 11 and Fig. 12. In both figures, we show the boundary of the region where there will be an observable signal in the corresponding dark matter detection channel: the signal *will be detectable* in the direction indicated by the arrows. In Fig. 11 we show results for those detection techniques for which the reach is mainly determined by the local dark matter density and average circular velocity at the Sun location (here assumed to respectively be $\rho_{DM}(r_0) = 0.38 \text{ GeV cm}^{-3}$ and $\bar{v}(r_0) = 221 \text{ km s}^{-1}$) and is relatively less sensitive to the *dark matter halo* profile, namely direct detection and the flux of energetic neutrinos from the center of the Sun originated by neutralino annihilations. In Fig. 12 we collect, instead, those quantities whose dependence on the details of the dark matter halo is more critical, namely antimatter fluxes from neutralino annihilations in the galactic halo. For the latter, we adopt the Adiabatically Contracted N03 Halo model[42]. We do not show the sensitivity contours for GLAST, since with this choice for the dark matter halo profile all of the parameter space is within the reach of the space-borne gamma-ray detector.

We notice that while the prospects for *Stage-2* detectors do not look particularly promising in this context, with the possible exception of small regions at low neutralino masses and with light scalars, next generation *Stage-3* detectors will have a sensitivity which we estimate to be able to cover most of the parameter space of the models under consideration. The sensitivity of IceCube will be instead critically dependent on the higgsino fraction of the lightest neutralino, which not only controls the pair annihilation cross section, but, more critically, sets the spin-dependent neutralino-nucleon scattering cross section. The reach contour we find follows in fact quite closely the LSP higgsino fraction. However, close to the boundary of the LEP excluded region at the bottom of frames *a*) and *b*), the neutralino mass is so low that the annihilation neutrinos are not energetic enough to give the required muon flux above the IceCube detection threshold.

Turning to antimatter searches, we assess here the Pamela sensitivity for primary antiproton and positron fluxes following the approach of Ref. [45], evaluating the projected total χ^2 and demanding a statistically significant (at 95% C.L.) excess over the estimated background.⁵ In Fig. 12, we shade in grey those regions which are already statistically excluded at the 95% C.L. by current data on the antiproton fluxes, when combined with an independently estimated secondary and tertiary background [45]. We stress though that this exclusion is very sensitive to the assumed halo profile, so is by no means a rigorous bound. In general, we find the most promising antimatter search technique will be the antiproton channel; remarkably enough, within this scenario we expect a signal at space-based antiprotons searches for neutralino masses as large as 0.5 TeV. A low-energy antideuteron signal is also expected at GAPS even on a balloon-borne experiment in a quite large portion of the parameter space. Finally, a significant positron signal can be

⁵Specifically, we evaluate the Pamela sensitivity on the $(m_0, m_{1/2})$ planes using the approach of Ref. [45], where the authors evaluate a prospective χ^2 taking into account a background independently computed with the Galprop package [72] and an estimated energy binning [73]. This approach is more accurate than looking at a single energy bin, although it has been checked that the two approaches are in reasonable agreement.

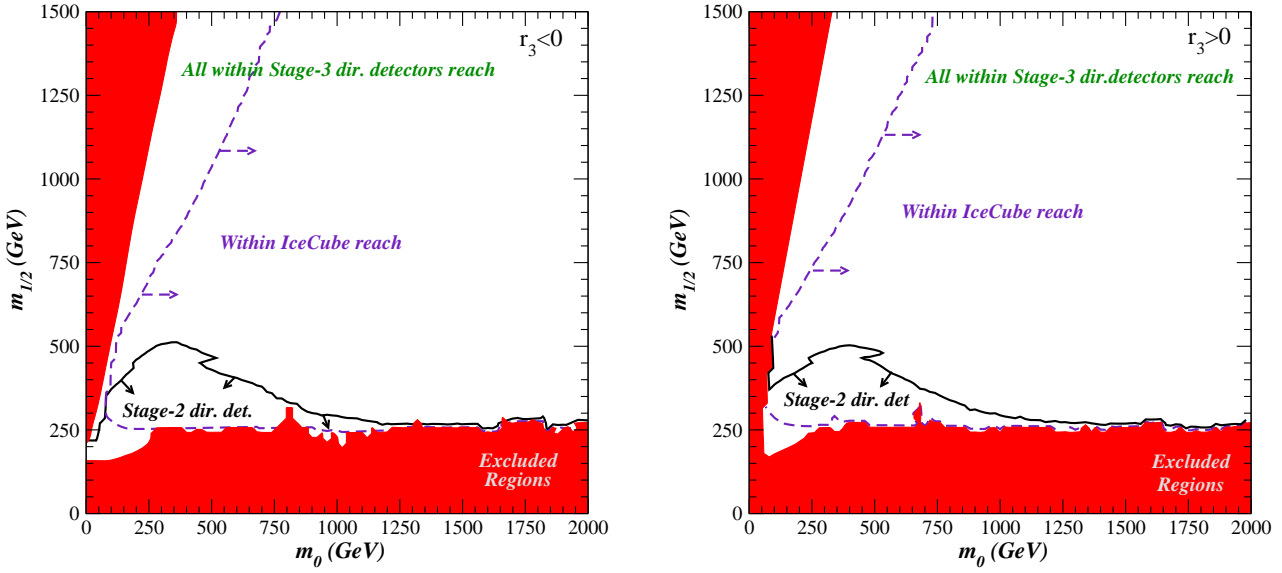


Figure 11: Projections for the reach of Stage-2 and Stage-3 direct detection experiments, and of IceCube in the $(m_0, m_{1/2})$ planes of the LM3DM model with $r_3 < 0$ (left) and $r_3 > 0$ (right). We shade in red regions where the stau is lighter than the LSP, where electromagnetic gauge invariance is spontaneously broken, or where the lightest chargino mass is not compatible with the LEP-II bound. The arrows denote the regions where the signal should be detectable.

only marginally reconciled with current constraints from antiprotons, and might take place in the low scalar masses portion of the planes under scrutiny here.

We notice that in general the anti-particle sensitivity contours we obtain trace the higgsino fraction of the LSP: for very small values of m_0 , the sensitivity drops at lower neutralino masses even though the antimatter primary fluxes approximately scale as $\langle\sigma v\rangle/m_{\tilde{Z}_1}^2$, because the LSP becomes more bino-like. Notice also the corridor around $m_{1/2} = 400$ –450 GeV where the current anti-proton searches do not exclude the model. For smaller values of $m_{1/2}$, the LSP mass is small and the anti-proton flux is too large. This flux falls below the 95% CL limit until the LSP mass becomes large enough so that annihilation to $t\bar{t}$ becomes kinematically allowed, once again yielding a large anti-proton rate. Finally, when $m_{1/2}$ gets larger, the LSP mass increases, and the anti-particle rate once again drops below the current experimental limit.

We stress that the exclusion limits shown in frames *c*) and *d*) as well as the projections for the reach via anti-particle and gamma ray searches *are sensitive to our assumption of the adiabatically contracted N03 halo profile* which yields considerably higher values for anti-particle, and especially, gamma ray fluxes. Assuming different but equally viable galactic DM halo distributions [43, 44, 45, 13] modifies this conclusion. Until the halo profile can be independently determined, we believe that exploration of independent signals even in these “halo-profile-dependent excluded regions” should continue.

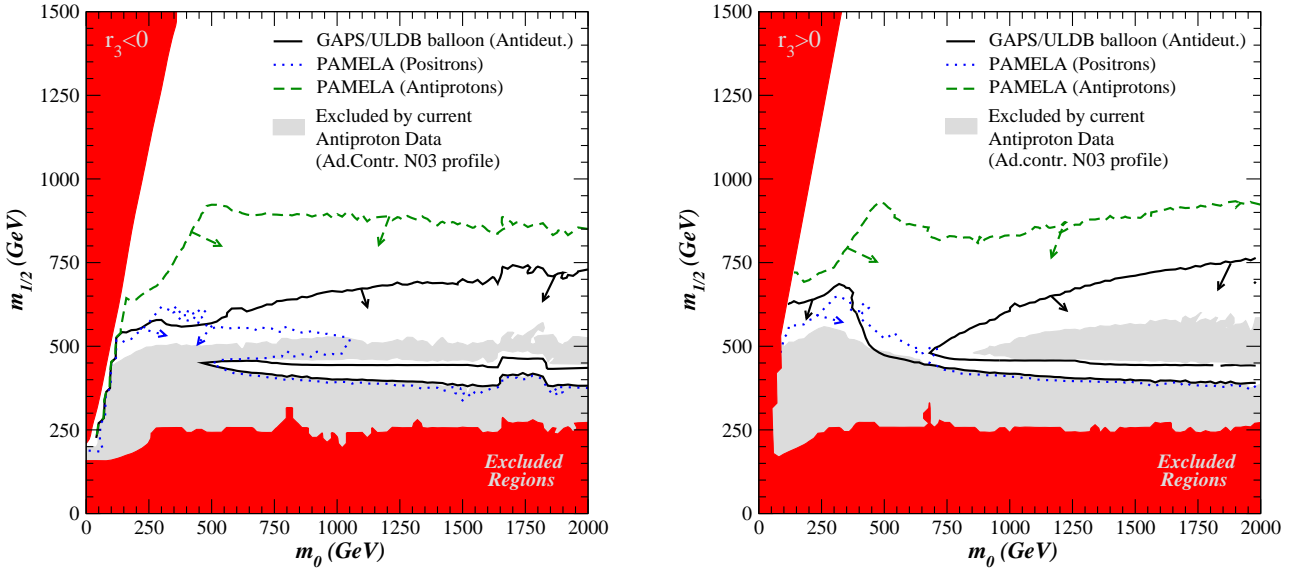


Figure 12: The same as Fig. 11, but for antimatter searches at PAMELA and GAPS. GLAST will have the sensitivity to probe the entire plane. These projections are sensitive to our choice of the adiabatically contracted N03 halo model for the distribution of the galactic dark matter. The regions shaded in grey are excluded by current antiproton data, again assuming the adiabatically contracted N03 halo model, but not necessarily for other equally viable halo profiles.

4. LM3DM at colliders

4.1 Fermilab Tevatron

In SUSY models with gaugino mass unification, the ratio of weak scale gaugino masses is typically found to be $M_1 : M_2 : M_3 \sim 1 : 2 : 7$. In the mSUGRA model, since $m_{\widetilde{W}_1} \sim M_2$ and $m_{\widetilde{g}} \sim M_3$, the bound on chargino masses $m_{\widetilde{W}_1} > 103.5$ GeV from LEP2 implies as well that $m_{\widetilde{g}} \gtrsim 350$ GeV. Since a 400 GeV gluino is typically beyond the reach of Fermilab Tevatron experiments, this leaves a relatively tiny window for a gluino discovery at the Tevatron, at least within the mSUGRA framework[74].⁶

However, in the case of LM3DM, the gluino mass can be much reduced relative to the value of $m_{\widetilde{W}_1}$. The situation is illustrated in Fig. 13, where we plot contours of $m_{\widetilde{g}}$ in the same m_0 vs. $m_{1/2}$ plane as in Fig. 5 where r_3 has been dialed to low enough values that the value of $\Omega_{\widetilde{Z}_1} h^2 = 0.11$ everywhere. Of importance here is that the gluino mass immediately adjacent to the blue-shaded LEP2 excluded region reaches values below 200 GeV, which is surely accessible to Fermilab Tevatron searches. In fact, for $m_0 = 1500$ GeV, $m_{1/2} = 250$ GeV, we find the LM3DM spectrum labelled as LM3DM3 in Table 1, where $m_{\widetilde{g}} = 183$ GeV is consistent with LEP lower limits on the chargino mass. In this scenario, the cross section for $p\bar{p} \rightarrow \tilde{g}\tilde{g}$ at the Fermilab Tevatron with $\sqrt{s} = 2$ TeV is ~ 21.5 pb, so that for 1 fb^{-1} of integrated luminosity, we already expect in excess of 20K $\tilde{g}\tilde{g}$ events!

⁶For $m_{\widetilde{g}} = 400$ GeV and $m_{\widetilde{q}} = 2m_{\widetilde{g}}$, we find $\sigma(p\bar{p} \rightarrow \tilde{g}\tilde{g}) = 27.8$ fb at $\sqrt{s} = 2$ TeV.

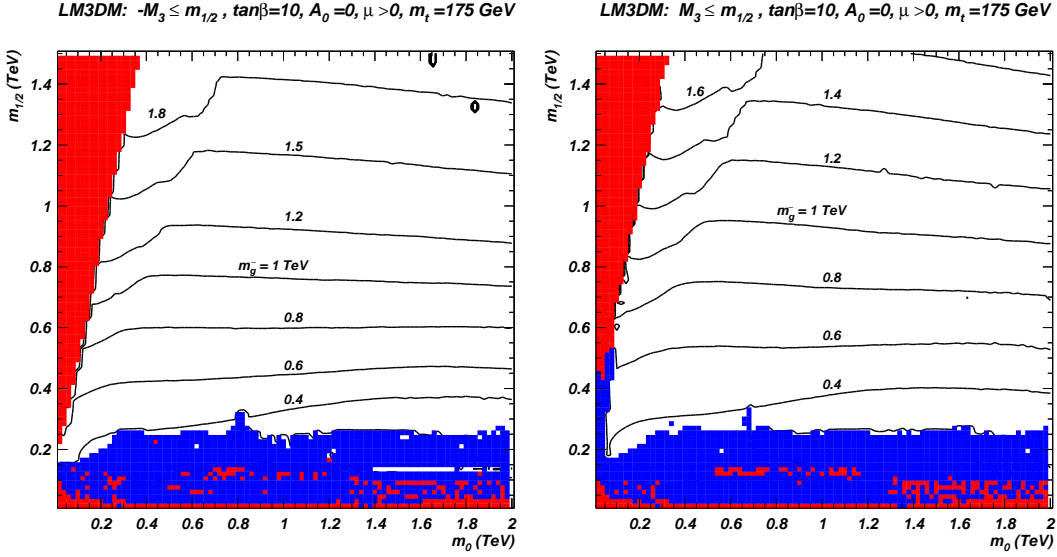


Figure 13: Contours of $m_{\tilde{g}}$ in the m_0 vs. $m_{1/2}$ plane for $\tan\beta = 10$, $A_0 = 0$, $\mu > 0$ and *a*) mSUGRA model, *b*) $M_3 < 0$ LM3DM and *c*) $M_3 > 0$ LM3DM.

Thus, considerable portions of the m_0 vs. $m_{1/2}$ parameter plane *that could not be probed at LEP* in the LM3DM scenario should be accessible to present day Tevatron SUSY searches!

Once the gluino pairs are produced, it is important to examine their decay modes. Inspection of the Isajet decay table for point LM3DM3 shows the surprising result that in this region of parameter space, gluino decays via three body modes $\tilde{g} \rightarrow q\bar{q}\tilde{Z}_i$ and $\tilde{g} \rightarrow q\bar{q}'\tilde{W}_j$ are suppressed, and that in fact the loop decays $\tilde{g} \rightarrow \tilde{Z}_i g$ are dominant! This large enhancement of the radiative decay relative to three body decays is not hard to understand. It has long been known[75] that, because of the tracelessness of the diagonal generators of the electroweak gauge group, for degenerate squarks, *all* contributions from the *gaugino components* of the neutralino cancel in the amplitude for the decay $\tilde{g} \rightarrow g\tilde{Z}_i$. As a result, unless $\tan\beta$ is very large, top squark loops completely dominate the radiative decay amplitude. The usual three-body decays of gluinos, on the other hand, receive significant contributions from the gaugino components of neutralinos, and indeed dominate these decays unless $\tan\beta$ is very large. For very heavy squarks, neglecting bottom quark Yukawa couplings and phase space effects, we find that

$$\frac{\Gamma(\tilde{g} \rightarrow g\tilde{Z}_i)}{\Gamma(\tilde{g} \rightarrow q\bar{q}\tilde{Z}_i)} = \frac{12}{\pi} \frac{\alpha_s f_t^2}{\left|A_{\tilde{Z}_i}^q\right|^2 + \left|B_{\tilde{Z}_i}^q\right|^2} |v_1^{(i)}|^2 \left(\frac{m_t}{m_{\tilde{g}}}\right)^2 \left(\frac{m_{\tilde{q}}}{m_{\tilde{t}}}\right)^4 \left(\ln \frac{m_{\tilde{t}}^2}{m_{\tilde{q}}^2} - 1\right)^2, \quad (4.1)$$

where, in the notation of Ref. [27], $A_{\tilde{Z}_i}^q$ and $B_{\tilde{Z}_i}^q$ are couplings of the i^{th} neutralino (gaugino components) to the quark-squark system, and $v_1^{(i)}$ is the component of the higgsino field \tilde{h}_u (that couples to up type (s)fermions) in this neutralino. In deriving (4.1), we have assumed that the $v_1^{(i)2} \ll \max(v_3^{(i)2}, v_4^{(i)2})$, *i.e.* that the neutralino is mainly gaugino-like. In many

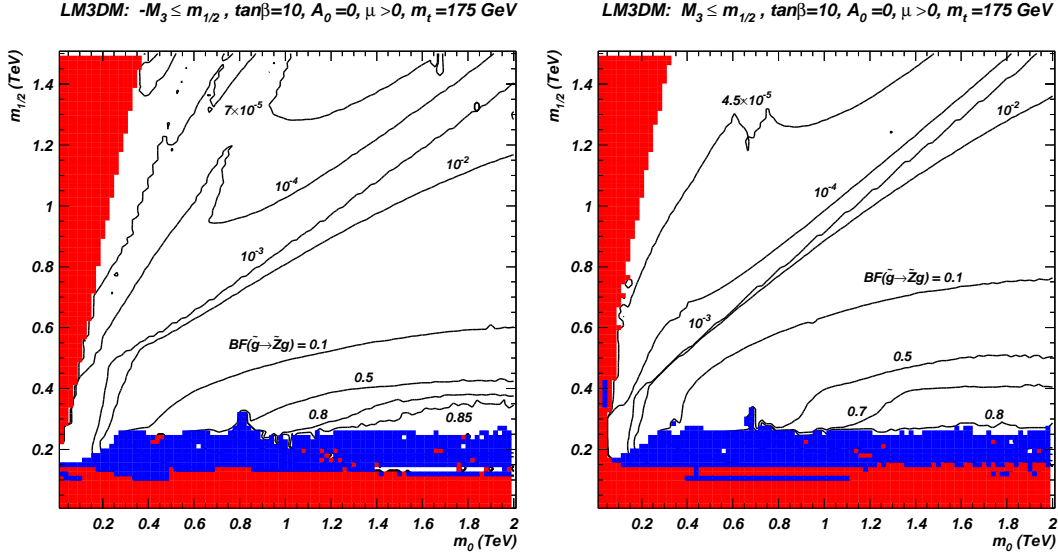


Figure 14: Contours of $BF(\tilde{g} \rightarrow \tilde{Z}_i g)$ (summed over $i = 1 - 4$) in the m_0 vs. $m_{1/2}$ plane for $\tan \beta = 10$, $A_0 = 0$, $\mu > 0$ and a) $M_3 < 0$ LM3DM and b) $M_3 > 0$ LM3DM.

models, where light neutralinos have only small higgsino components, gluino radiative decays have very small branching ratios because of the factor $v_1^{(i)2}$ in (4.1). This same factor is, however, precisely the reason for the large branching fraction in the LM3DM3 scenario that we have been discussing.

To bring home this point, we show in Fig. 14 the $\tilde{g} \rightarrow \tilde{Z}_i g$ branching fraction contours summed over $i = 1 - 4$ in the m_0 vs. $m_{1/2}$ plane of Fig. 5. We see in the lower right region where gluino masses are quite light that the cumulative gluino loop decay branching exceeds 80%! Thus, in this region, $\tilde{g}\tilde{g}$ production events with $\tilde{g} \rightarrow \tilde{Z}_1 g$ will give rise typically to dijet+ E_T^{miss} events, much like squark pair production when $m_{\tilde{q}} < m_{\tilde{g}}$. However, the $\tilde{g} \rightarrow \tilde{Z}_i g$ decays are not only into $g\tilde{Z}_1$, but also have large rates into $\tilde{Z}_2 g$ and $\tilde{Z}_3 g$, as shown in Fig. 15, where these branching fractions are plotted versus m_0 for fixed $m_{1/2} = 300$ GeV and other parameters as in Fig. 13.

The \tilde{Z}_2 and \tilde{Z}_3 which are produced either directly or via gluino cascade decays will likely decay via three-body modes which, if $m_{\tilde{q}}$ is large enough, are dominated by Z exchange. The $m_{\tilde{Z}_2} - m_{\tilde{Z}_1}$ mass gap is shown in Fig. 16. Since $|\mu|$ is typically quite low, and the lighter \tilde{Z}_i are mixed higgsino states, this mass gap varies in the 30-70 GeV range when \tilde{Z}_1 is MHDM, so that $\tilde{Z}_2 \rightarrow \ell\ell\tilde{Z}_1$ (and also frequently $\tilde{Z}_3 \rightarrow \ell\ell\tilde{Z}_1$) occur all over the MHDM portion of the LM3DM parameter space. In this case, one or possibly even two distinct $m(\ell^+\ell^-)$ mass edges should be apparent if enough sparticle pair production events are generated. The $m(\ell^+\ell^-)$ mass edges of course are renowned for being the starting point for sparticle mass reconstruction at hadron colliders[76].

4.2 CERN LHC

When comparing the LM3DM scenario to the mSUGRA model, we have found that for a given point in the m_0 vs. $m_{1/2}$ plane, gluino and squark masses are quite suppressed

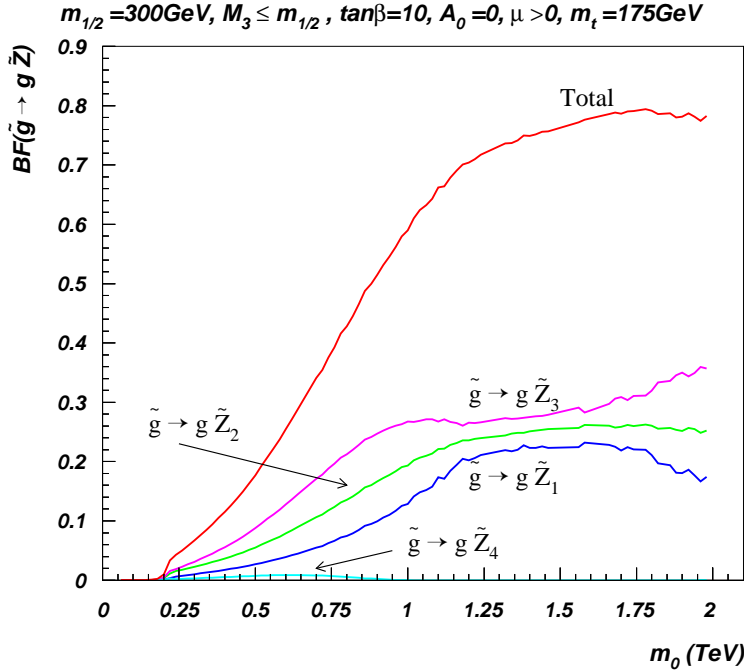


Figure 15: A plot of $BF(\tilde{g} \rightarrow \tilde{Z}_i g)$ (for $i = 1 - 4$) versus m_0 for $m_{1/2} = 300$ GeV, $A_0 = 0$, $\tan \beta = 10$, $\mu > 0$ where at each point M_3 has been dialed so that $\Omega_{\tilde{Z}_1} h^2 = 0.11$

relative to slepton masses and somewhat suppressed relative to chargino masses. The upshot is that sparticle production at the LHC should be even more dominated by gluino and squark production (compared to other sparticle production reactions) than in the case of mSUGRA. Indeed, for the points listed in Table 1 we find $\sigma(pp \rightarrow \tilde{g}\tilde{g}X) = 2, 84, 31$ and 4760 pb, for mSUGRA, LM3DM1, LM3DM2 and LM3DM3, respectively. The signatures from gluino and squark pair production at the LHC from LM3DM will consist of various multi-jet plus multi-lepton plus E_T^{miss} events as in mSUGRA[77]. However, in the lower right portion of the m_0 vs. $m_{1/2}$ plane, the SUSY events should consist mainly of dijet + E_T^{miss} events when $\tilde{g} \rightarrow \tilde{Z}_1 g$, with additional jets and opposite sign/same flavor (OS/SF) dilepton events coming from $\tilde{g} \rightarrow \tilde{Z}_2 g$ or $\tilde{Z}_3 g$ followed by \tilde{Z}_2 or \tilde{Z}_3 decay. In particular, same sign dileptons, which are somewhat characteristic of gluino pair production[78], will be relatively suppressed when the gluino loop decays are dominant.

The LHC reach for SUSY in the mSUGRA model has been calculated in Ref. [79, 80] assuming 100 fb^{-1} of integrated luminosity. The ultimate reach of the LHC is mainly dependent on the value of $m_{\tilde{g}}$ and $m_{\tilde{q}}$, and not so dependent on their particular decay modes. Thus, we may translate the mSUGRA reach results into contours into the $m_{\tilde{g}}$ vs. $m_{\tilde{g}}$ plane, and then convert this contour into a reach contour in the m_0 vs. $m_{1/2}$ plane of the LM3DM scenario. The translated reach contour is shown in Fig. 17 for the same parameters as in Fig. 5b). The reach contour on the left portion of the plot in the BDM region mainly follows the $m_{\tilde{g}} \simeq m_{\tilde{q}} \simeq 3$ TeV contour. The upper left increase in reach is due to the sliver of MHDM region at low m_0 and large $m_{1/2}$ shown in Fig. 5b), where r_3 is relatively

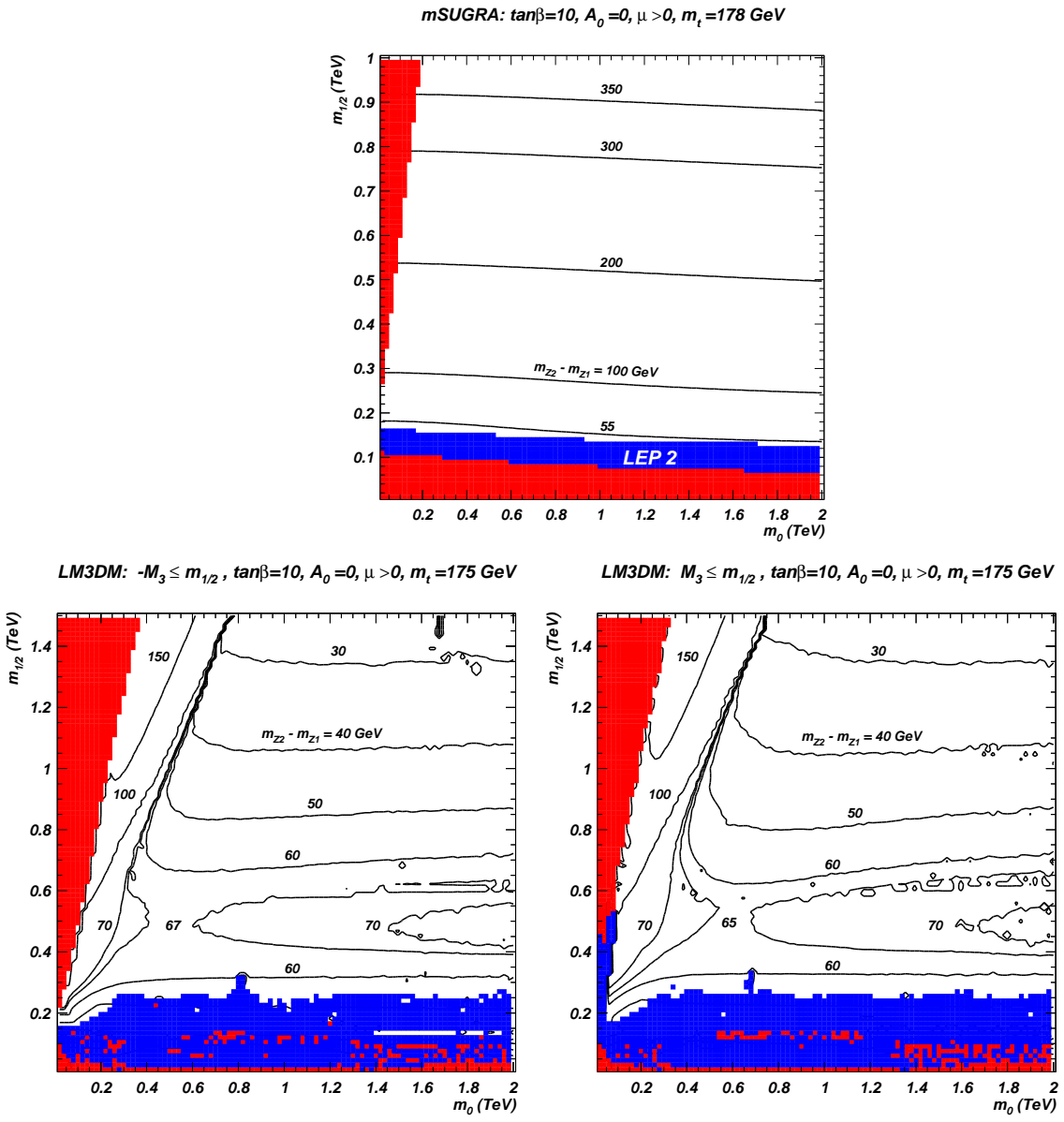


Figure 16: Contours of $m_{\tilde{Z}_2} - m_{\tilde{Z}_1}$ mass gap in the m_0 vs. $m_{1/2}$ plane for $\tan\beta = 10$, $A_0 = 0$, $\mu > 0$ in the case of a) the mSUGRA model, b) $M_3 < 0$ LM3DM and c) $M_3 > 0$ LM3DM.

reduced. At intermediate m_0 , neutralino annihilation is assisted by the A resonance, and so higher r_3 values are found to match the WMAP constraint (recall in this region the \tilde{Z}_1 is bino-like). On the right hand side of the plot for $m_0 > 1.2$ TeV, we are in the MHDM region with lower r_3 values, and consequently lighter gluino and squark masses. Thus, the reach is increased. At very large m_0 values, $m_{\tilde{q}} > m_{\tilde{g}}$, and here the LHC reach extends only out to $m_{\tilde{g}} \sim 2.7$ TeV. We should mention that since light neutralinos and chargino have significant higgsino component in the LM3DM scenario, gluino decays to the third generation quarks will be enhanced exactly as in the FP/HB region of the mSUGRA model,

so that b -jet tagging may improve the LHC reach by $\sim 10 - 15\%$ beyond that shown in the figure.[81]

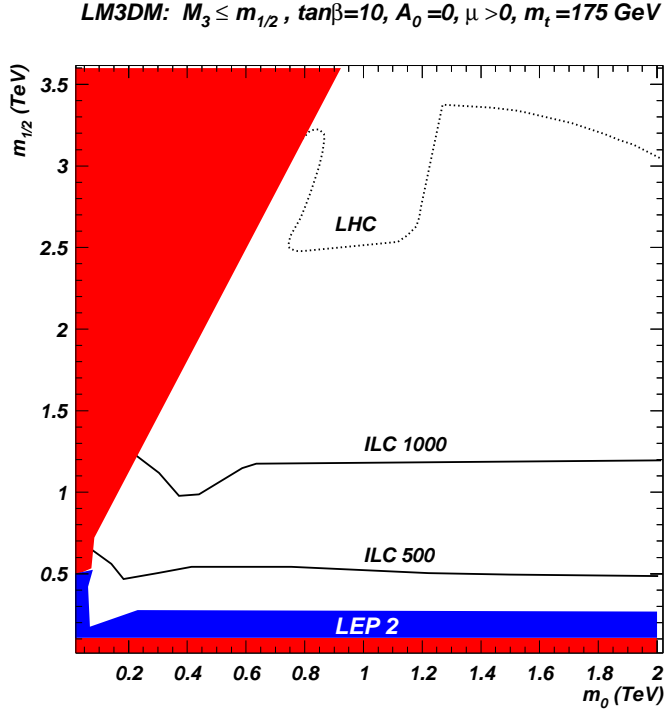


Figure 17: Reach contours for the CERN LHC with 100 fb^{-1} of integrated luminosity and for a $\sqrt{s} = 0.5$ and 1 TeV linear e^+e^- collider in the m_0 vs. $m_{1/2}$ plane for $\tan \beta = 10$, $A_0 = 0$, $\mu > 0$ and where M_3 has been reduced such that $\Omega_{\tilde{Z}_1} h^2 = 0.11$ at every point in the plane.

For SUSY searches at the CERN LHC, Hinchliffe *et al.* have pointed out[82] that an approximate value of $m_{\tilde{q}}$ or $m_{\tilde{g}}$ can be gained by extracting the maximum in the M_{eff} distribution, where $M_{eff} = E_T^{\text{miss}} + E_T(\text{jet 1}) + E_T(\text{jet 2}) + E_T(\text{jet 3}) + E_T(\text{jet 4})$. Their analysis will carry over to much of the LM3DM scenario,⁷ as well as in models with gaugino mass unification, so that the approximate mass scale of strongly interacting sparticles will be known soon after a supersymmetry signal has been established.

In mSUGRA, a dilepton mass edge should be visible in SUSY signal events only if $m_{1/2} \lesssim 250 \text{ GeV}$ (where $\tilde{Z}_2 \rightarrow \tilde{Z}_1 \ell \bar{\ell}$ is allowed) or if two body $\tilde{Z}_2 \rightarrow \ell \bar{\ell}$, $\tilde{\ell} \bar{\ell}$ decays are allowed. In the case of LM3DM, as with MWDM[22] and BWCA DM[23], the dilepton mass edge should be visible over almost all parameter space. We illustrate the situation for three of the case studies listed in Table 1.⁸ The first case, labeled mSUGRA, has

⁷An exception is the low $m_{1/2}$, large m_0 region of Fig. 5 where dijet production is instead dominant.

⁸In this study, a toy detector simulation is employed with calorimeter cell size $\Delta\eta \times \Delta\phi = 0.05 \times 0.05$ and $-5 < \eta < 5$. The hadronic energy resolution is taken to be $80\%/\sqrt{E}$ for $|\eta| < 2.6$ and $100\%/\sqrt{E}$ for $|\eta| > 2.6$. The electromagnetic energy resolution is assumed to be $3\%/\sqrt{E}$. We use a UA1-like jet finding algorithm with jet cone size $R = 0.5$ and $p_T^{\text{jet}} > 25 \text{ GeV}$. We also require that $|\eta_\ell| < 2.5$ and $|\eta_j| < 3$. Leptons (es or μ s) have to also satisfy $p_T^{\text{lepton}} \geq 10 \text{ GeV}$. Leptons are considered isolated if the visible activity within the cone $\Delta R < 0.3$ is $\Sigma E_T^{\text{cells}} < 2 \text{ GeV}$. The strict isolation criterion helps reduce multi-lepton background from heavy quark (especially $t\bar{t}$) production.

$m_0 = m_{1/2} = 300$ GeV, with $A_0 = 0$, $\tan \beta = 10$ and $\mu > 0$. In this case, $\tilde{g}\tilde{g}$, $\tilde{g}\tilde{q}$ and $\tilde{q}\tilde{q}$ production occurs with a combined cross section of about 12 pb, while the total SUSY cross section is around 13.4 pb (the additional 1.4 pb comes mainly from -ino pair production and -ino-squark or -ino-gluino associated production). The case of LM3DM1, with $M_3 = 150$ GeV, has a total cross section of 215 pb. The case of LM3DM2, with slightly heavier squark and gluino masses, has a total production cross section of 101 pb. The special case of LM3DM3, which should be accessible to Tevatron searches via its light gluino, has a total SUSY cross section at LHC of 3744 pb.

We have generated 750K LHC SUSY events for the cases LM3DM1 and LM3DM2 using Isajet 7.73, and passed them through a toy detector simulation as described above. We adopt cuts which are similar to those of LHC point 5 of the study of Hinchliffe *et al.*[82], which efficiently select the SUSY signal while essentially eliminating SM backgrounds: $E_T^{\text{miss}} > \text{max}(100 \text{ GeV}, 0.2M_{\text{eff}})$, at least four jets with $E_T > 50$ GeV, where the hardest jet has $E_T > 100$ GeV, transverse sphericity $S_T > 0.2$ and $M_{\text{eff}} > 800$ GeV.

In these events, we require at least two isolated leptons, and then plot the invariant mass of all same flavor/opposite sign dileptons. The results are shown in Fig. 18. In the case of the mSUGRA model, frame *a*), there is a sharp peak at $m(\ell^+\ell^-) \sim M_Z$, which comes from $\tilde{Z}_2 \rightarrow \tilde{Z}_1 Z^0$ decays where \tilde{Z}_2 is produced in the gluino and squark cascade decays. In the case of LM3DM1 in frame *b*), we clearly see a continuum distribution with a mass edge at $m(\ell^+\ell^-) < m_{\tilde{Z}_2} - m_{\tilde{Z}_1} = 58.5$ GeV. We also see events beyond this edge along with a peak at M_Z . In this case, $m_{\tilde{Z}_3} - m_{\tilde{Z}_1} = 90.3$ GeV is within Γ_Z of M_Z and we would expect that dileptons from $\tilde{Z}_3 \rightarrow \tilde{Z}_1 \ell\bar{\ell}$ decays have their mass sharply peaked just below M_Z . This peak would also be populated by Z bosons produced via $\tilde{Z}_4 \rightarrow \tilde{Z}_i Z^0$ or $\tilde{W}_2 \rightarrow \tilde{W}_1 Z^0$ decays. The cross section plotted here is ~ 188 fb, which would correspond to 19K events in 100 fb^{-1} of integrated luminosity (the sample shown in the figure contains just 646 events). In frame *c*)—with a cross section of ~ 207 fb (but just 1550 actual entries)—once again we see the Z^0 peak from decays of heavier charginos and neutralinos to the Z boson, together with a mass edge at $m(\ell^+\ell^-) < m_{\tilde{Z}_2} - m_{\tilde{Z}_1} = 61$ GeV, and a continuum in between, presumably mainly from chargino pairs in SUSY events. In both these LM3DM cases, the $m_{\tilde{Z}_2} - m_{\tilde{Z}_1}$ mass edge should be very precisely measurable. It should also be clear that this edge is inconsistent with models based on gaugino mass unification, in that the projected ratios $M_1 : M_2 : M_3$ will not be in the order $1 : \sim 2 : \sim 7$ as in mSUGRA. Although the $\tilde{Z}_2 - \tilde{Z}_1$ mass edge will be directly measurable, the absolute neutralino and chargino masses will, as usual, be more difficult to extract at the LHC.

4.3 Linear e^+e^- collider

The reach of the CERN LHC for supersymmetric matter is determined mainly by $m_{\tilde{q}}$ and $m_{\tilde{g}}$, which depend on m_0 and M_3 . In contrast, the reach of the ILC for SUSY is largely determined by whether or not the reactions $e^+e^- \rightarrow \tilde{W}_1^+\tilde{W}_1^-$ or $e^+e^- \rightarrow \tilde{\ell}^+\tilde{\ell}^-$ are kinematically accessible[83]. For instance, chargino pair production is expected to be visible if $\sqrt{s} > 2m_{\tilde{W}_1}$. The value of $m_{\tilde{W}_1}$ depends mainly on M_2 and μ . Thus, in the LM3DM scenario where M_1 and M_2 take values similar to mSUGRA, but where μ is quite small, the reach of the ILC in the m_0 vs. $m_{1/2}$ plane via chargino pair production will be

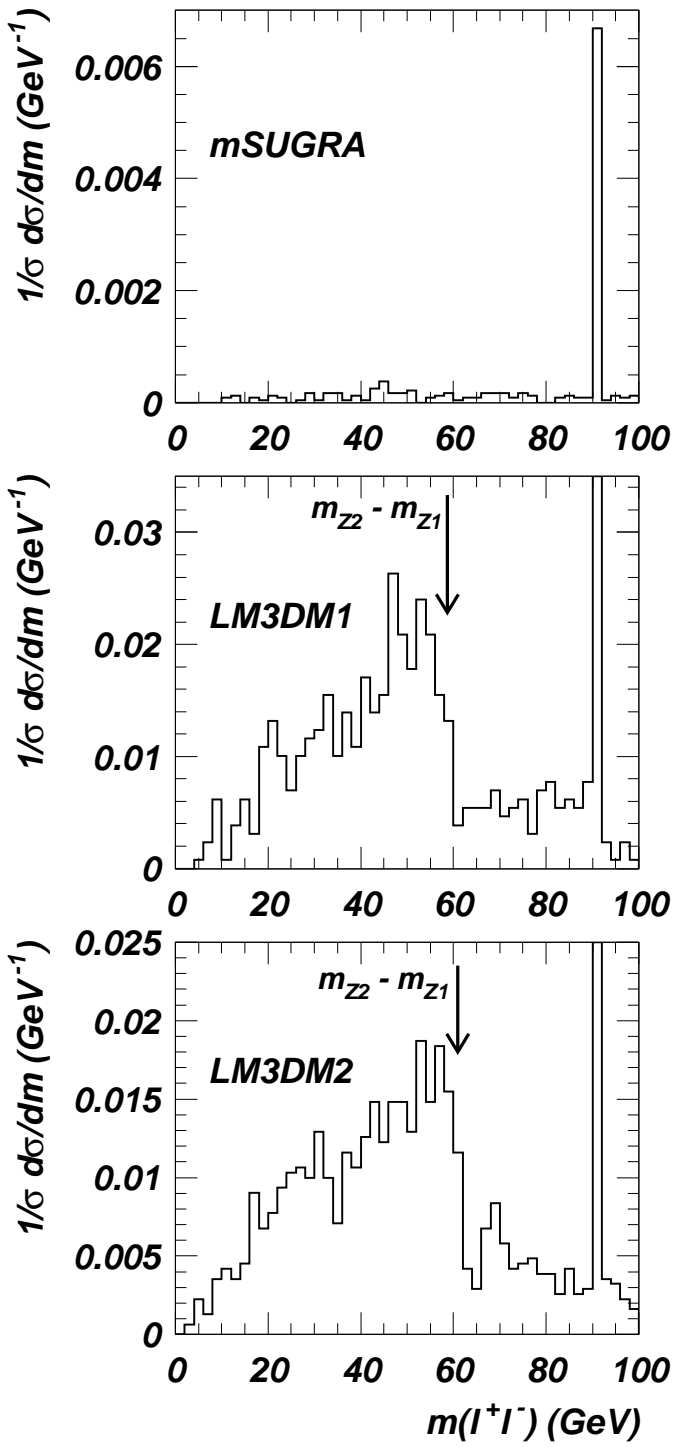


Figure 18: Distribution of same flavor/opposite sign dileptons from SUSY events at the CERN LHC from *a)* mSUGRA, *b)* LM3DM1 and *c)* LM3DM2 cases as in Table 1.

enhanced relative to the case of the mSUGRA model. Since slepton masses are relatively unaffected by lowering M_3 , the ILC reach for slepton pair production will be similar to

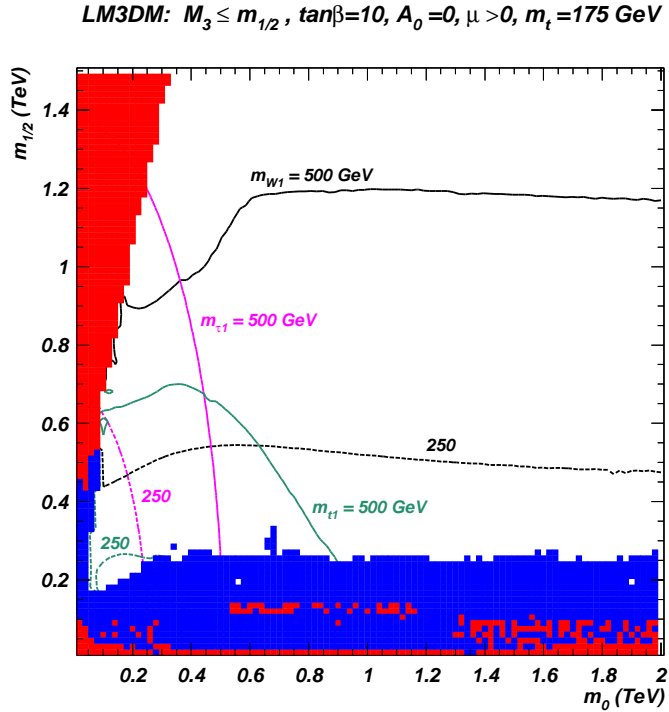


Figure 19: Reach of the ILC for SUSY in the LM3DM scenario where M_3 is lowered until $\Omega_{\tilde{Z}_1} h^2 = 0.11$ at every point in the m_0 vs. $m_{1/2}$ plane. We show the ILC reach for $\sqrt{s} = 0.5$ TeV and 1 TeV via the kinematic limits for $\tilde{W}_1^+ \tilde{W}_1^-$, $\tilde{\tau}^+ \tilde{\tau}^-$ and $\tilde{t}_1 \tilde{t}_1$ production.

the mSUGRA case. In addition, squark masses are relatively suppressed in the LM3DM scenario, especially the top squark, so that there will be a non-trivial reach of the ILC for $\tilde{t}_1 \tilde{t}_1$ production. The situation is illustrated in Fig. 19 where we show the ultimate reach of the ILC in the m_0 vs. $m_{1/2}$ plane for $\tan\beta = 10$, $A_0 = 0$, $\mu > 0$ and $m_t = 175$ GeV. We have dialed M_3 at every point to give $\Omega_{\tilde{Z}_1} h^2 = 0.11$, in accord with the WMAP observation. The reach of ILC with $\sqrt{s} = 0.5$ TeV is denoted by dashed contours, and extends to $m_{1/2} \sim 500$ GeV, while the corresponding reach within the mSUGRA framework with gaugino mass unification extends to $m_{1/2} \sim 320$ GeV[83]. The reach of ILC with $\sqrt{s} = 1$ TeV extends to $m_{1/2} \sim 1 - 1.2$ TeV, compared with the mSUGRA value of $m_{1/2} \sim 600$ GeV. The combined reach (from chargino and selectron production) of the $\sqrt{s} = 0.5$ and 1 TeV ILC relative to the LHC are shown in Fig. 17. The LHC reach is always larger than that of the ILC, primarily because of the relative reduction of gluino and squark masses in the LM3DM framework.

The distinguishing feature of LM3DM is that the small μ parameter gives rise to a rather light spectrum of the two charginos and all four neutralinos. Thus, many more -ino pair production reactions are likely to be accessible to a linear $e^+ e^-$ collider than would occur in the mSUGRA model. As an example, we show in Table 2 the various SUSY cross sections in fb which are accessible to a $\sqrt{s} = 0.5$ TeV machine for the four case studies listed in Table 1. While only $\tilde{W}_1 \tilde{W}_1$, $\tilde{Z}_1 \tilde{Z}_2$ and $\tilde{Z}_2 \tilde{Z}_2$ production are possible in the mSUGRA

reaction	mSUGRA	LM3DM1	LM3DM2	LM3DM3
$W_1 W_1$	132.0	312.7	307.7	538.1
$\widetilde{W}_1 \widetilde{W}_2$	—	59.5	52.7	49.5
$\widetilde{Z}_1 \widetilde{Z}_2$	22.7	48.2	45.1	3.0
$\widetilde{Z}_1 \widetilde{Z}_3$	—	32.5	29.8	86.8
$\widetilde{Z}_1 \widetilde{Z}_4$	—	3.2	3.0	0.02
$\widetilde{Z}_2 \widetilde{Z}_2$	12.6	21.6	18.1	0.6
$\widetilde{Z}_2 \widetilde{Z}_3$	—	99.9	101.2	53.7
$\widetilde{Z}_2 \widetilde{Z}_4$	—	7.4	4.6	0.2
$\widetilde{Z}_3 \widetilde{Z}_3$	—	0.1	0.07	0.5
$\widetilde{Z}_3 \widetilde{Z}_4$	—	22.9	11.5	41.6

Table 2: Cross sections in fb for $e^+e^- \rightarrow SUSY$ processes at a $\sqrt{s} = 0.5$ TeV linear collider, for the four case studies listed in Table 1.

model, for the LM3DM scenarios all ten reactions listed are accessible at a $\sqrt{s} = 0.5$ TeV linear collider, although some of these have very low rates. It does appear though that every chargino and neutralino is produced via some reaction with cross section exceeding 10 fb. Detailed studies of the chargino-neutralino sector along the lines discussed in Ref. [84] should be feasible within the LM3DM scenario.

Another feature of LM3DM relevant to linear e^+e^- colliders is that the relatively low squark masses which are expected in this scenario means that squark pair production is more likely to be possible, especially for a $\sqrt{s} \geq 1$ TeV machine. In most cases, the decay $\tilde{q} \rightarrow \tilde{q}q$ is kinematically allowed, so that gluino production might be studied in the e^+e^- environment, since they can be produced via the cascade decays of the heavier squarks. In this case, very precise determination of squark and gluino masses may be possible if the end point of the energy spectrum of the primary quark jet in the decay $\tilde{q} \rightarrow q\tilde{q}$ can be identified.

5. Summary and conclusions

If we identify the relic density of CDM (1.1), with that of thermally produced LSPs of an R-parity conserving SUSY model, the WMAP measurement serves as a stringent constraint on any SUSY model. It is then interesting to explore the ramifications of this measurement, both for collider searches for supersymmetry, as well as for direct and indirect searches for DM at non-accelerator facilities. It is also necessary to explore just how robust these ramifications are to changes in the underlying SUSY framework that do not alter the successful prediction for the LSP relic density. In previous studies, we explored how the WMAP CMB constraint could be satisfied if (1) we relax the (phenomenologically unnecessary) assumption that the Higgs scalar mass parameters unify with sfermion mass parameters at high scales, and (2) if we relax the assumption of the unification of gaugino masses, and allow the ratio M_1/M_2 (which controls the composition of the LSP) to float freely. In this paper, we study the implications of what we dub as the low M_3 DM (LM3DM) model,

which is essentially the paradigm mSUGRA framework, except that the $SU(3)$ gaugino mass is allowed to adopt any value. Following earlier studies [25, 26] we find that, for m_0 values not hierarchically larger than $m_{1/2}$, the value of $|\mu|$ is reduced when the GUT scale gluino mass parameter $|M_3| < m_{1/2}$, and MHDM or BDM solutions become viable for essentially all values of model parameters.

The sizeable higgsino component of MHDM implies enhanced detection rates in ongoing, planned and proposed experiments searching for DM relative to the bino LSP case more typical in mSUGRA; see Fig. 11 and Fig. 12. While direct searches at stage 2 detectors such as CDMS2 can explore only a relatively limited portion of the parameter space, the entire parameter space should be explorable at the proposed stage 3 detectors typified by the SuperCDMS or 1-ton XENON experiments. Indirect searches via the detection of hard muon neutrinos from the core of the sun should also be possible at IceCube over much of the model parameter space. Experiments looking for anti-particles and gamma rays from the annihilation of neutralinos in our galactic halo should also be able to detect signals from MHDM. These projections should be interpreted with care because they are sensitive to the precise distribution of the DM in the galactic halo.

By comparing detection rates in direct and indirect search experiments, it is possible to qualitatively distinguish the MHDM scenario from scenarios where the dark matter is bino-like as in mSUGRA (either in the bulk region or in the Higgs resonance region) or with bino-wino coannihilation yielding the WMAP value, or mixed with the wino [23]. Experiments at colliders will be able to provide additional evidence in favor of one or the other of these scenarios.

MHDM, on the other hand, occurs in a variety of models. It may occur for very large values of m_0 in the HB/FP region of the mSUGRA model, in non-universal Higgs mass (NUHM) models where the GUT scale Higgs mass parameters are equal but larger than the corresponding sfermion parameters or in more general NUHM models, or, as we have just seen, in the LM3DM models. Distinction between these various MHDM scenarios is only possible via examination of the properties of *other* sparticles which are accessible via collider searches for SUSY.

The main distinguishing feature of the LM3DM model is that the ratio of coloured sparticle masses to those of colour singlet sleptons, charginos and neutralinos is smaller in the LM3DM model than in most other models. This clearly favours SUSY searches at hadron colliders such as the Fermilab Tevatron or the CERN LHC vis à vis searches at electron-positron colliders. For instance, while the LEP lower limit on the chargino mass greatly restricts the potential of the Fermilab Tevatron to discover gluinos within the mSUGRA framework (or, for that matter, in any framework with unification of gaugino masses), *Tevatron searches for gluinos may yet lead to the discovery of SUSY if SUSY is realized as in the LM3DM model*[85]. In this case, experiments at the LHC will have a reach much larger than that of even a TeV linear collider. Despite this, experiments at the linear collider will play a big role in elucidating the physics and allowing us to zero in on the underlying scenario. Since $|\mu|$ is comparable to the weak scale electroweak gaugino masses, it is likely that *all* charginos and neutralinos will be accessible and their properties measured at a TeV linear collider. In this case, it will be possible to directly determine M_1 ,

M_2 , μ and $\tan \beta$. Combining these with the determination of $m_{\tilde{g}}$ that should be possible at the LHC, we should be able to determine that the GUT scale gluino mass is smaller than the corresponding electroweak gaugino masses.⁹ If we are lucky, the top squark and perhaps even other squarks, may be kinematically accessible. In this case, the gluino may also be accessible as a decay product of the squarks, and true bottom-up sparticle spectroscopy would be possible.

Acknowledgments

This research was supported in part by the U.S. Department of Energy grant numbers DE-FG02-97ER41022, DE-FG03-94ER40833, DE-FG03-92-ER40701 and FG02-05ER41361, and by NASA grant number NNG05GF69G.

References

- [1] D. N. Spergel *et al.*, [astro-ph/0302209](#); C. L. Bennett *et al.*, [astro-ph/0302207](#).
- [2] H. Goldberg, *Phys. Rev. Lett.* **50** (1419) 1983; J. Ellis, J. Hagelin, D. Nanopoulos and M. Srednicki, *Phys. Lett.* **B127**, 233 (1983); J. Ellis, J. Hagelin, D. Nanopoulos, K. Olive and M. Srednicki, *Nucl. Phys.* **B238**, 453 (1984).
- [3] For recent reviews, see *e.g.* C. Jungman, M. Kamionkowski and K. Griest, *Phys. Rept.* **267** (1995) 1996; A. Lahanas, N. Mavromatos and D. Nanopoulos, *Int. J. Mod. Phys.* **D 12** (2003) 1529; M. Drees, [hep-ph/0410113](#); K. Olive, “Tasi Lectures on Astroparticle Physics”, [astro-ph/0503065](#).
- [4] J. Ellis, K. Olive, Y. Santoso and V. Spanos, *Phys. Lett.* **B 565** (2003) 176; H. Baer and C. Balazs, *JCAP* **05** (2003) 006; U. Chattapadhyay, A. Corsetti and P. Nath, *Phys. Rev.* **D 68** (2003) 035005; A. Lahanas and D. V. Nanopoulos, *Phys. Lett.* **B 568** (2003) 55; A. Djouadi, M. Drees and J. Kneur, [hep-ph/0602001](#); for a review, see A. Lahanas, N. Mavromatos and D. Nanopoulos, Ref. [3].
- [5] A. Chamseddine, R. Arnowitt and P. Nath, *Phys. Rev. Lett.* **49** (1982) 970; R. Barbieri, S. Ferrara and C. Savoy, *Phys. Lett.* **B 119** (1982) 343; N. Ohta, *Prog. Theor. Phys.* **70** (1983) 542; L. J. Hall, J. Lykken and S. Weinberg, *Phys. Rev.* **D 27** (1983) 2359; for reviews, see H. P. Nilles, *Phys. Rep.* **110** (1984) 1, and P. Nath, [hep-ph/0307123](#).
- [6] H. Baer and M. Brhlik, *Phys. Rev.* **D 53** (1996) 597; V. Barger and C. Kao, *Phys. Rev.* **D 57** (1998) 3131.
- [7] J. Ellis, T. Falk and K. Olive, *Phys. Lett.* **B 444** (1998) 367; J. Ellis, T. Falk, K. Olive and M. Srednicki, *Astropart. Phys.* **13** (2000) 181; M.E. Gómez, G. Lazarides and C. Pallis, *Phys. Rev.* **D 61** (2000) 123512 and *Phys. Lett.* **B 487** (2000) 313; A. Lahanas, D. V. Nanopoulos and V. Spanos, *Phys. Rev.* **D 62** (2000) 023515; R. Arnowitt, B. Dutta and Y. Santoso, *Nucl. Phys.* **B 606** (2001) 59; see also Ref. [39]
- [8] K. L. Chan, U. Chattopadhyay and P. Nath, *Phys. Rev.* **D 58** (1998) 096004. J. Feng, K. Matchev and T. Moroi, *Phys. Rev. Lett.* **84** (2000) 2322 and *Phys. Rev.* **D 61** (2000)

⁹It may be interesting to examine whether this can also be concluded from the determination of two or more dilepton mass edges from the decay of neutralinos at the LHC.

075005; see also H. Baer, C. H. Chen, F. Paige and X. Tata, *Phys. Rev. D* **52** (1995) 2746 and *Phys. Rev. D* **53** (1996) 6241; H. Baer, C. H. Chen, M. Drees, F. Paige and X. Tata, *Phys. Rev. D* **59** (1999) 055014; for a model-independent approach, see H. Baer, T. Krupovnickas, S. Profumo and P. Ullio, *J. High Energy Phys.* **0510** (2005) 020.

[9] M. Drees and M. Nojiri, *Phys. Rev. D* **47** (1993) 376; H. Baer and M. Brhlik, *Phys. Rev. D* **57** (1998) 567; H. Baer, M. Brhlik, M. Diaz, J. Ferrandis, P. Mercadante, P. Quintana and X. Tata, *Phys. Rev. D* **63** (2001) 015007; J. Ellis, T. Falk, G. Ganis, K. Olive and M. Srednicki, *Phys. Lett. B* **510** (2001) 236; L. Roszkowski, R. Ruiz de Austri and T. Nihei, *J. High Energy Phys.* **0108** (024) 2001; A. Djouadi, M. Drees and J. L. Kneur, *J. High Energy Phys.* **0108** (2001) 055; A. Lahanas and V. Spanos, *Eur. Phys. J. C* **23** (2002) 185.

[10] R. Arnowitt and P. Nath, *Phys. Rev. Lett.* **70** (1993) 3696; H. Baer and M. Brhlik, Ref. [6]; A. Djouadi, M. Drees and J. Kneur, *Phys. Lett. B* **624** (2005) 60.

[11] C. Böhm, A. Djouadi and M. Drees, *Phys. Rev. D* **30** (2000) 035012; J. R. Ellis, K. A. Olive and Y. Santoso, *Astropart. Phys.* **18** (2003) 395; J. Edsjö, *et al.*, *JCAP* **04** (2003) 001

[12] H. Baer, A. Belyaev, T. Krupovnickas and A. Mustafayev, *J. High Energy Phys.* **0406** (2004) 044.

[13] H. Baer, A. Mustafayev, S. Profumo, A. Belyaev and X. Tata, *Phys. Rev. D* **71** (2005) 095008 and *J. High Energy Phys.* **0507** (2005) 065.

[14] D. Auto, H. Baer, A. Belyaev and T. Krupovnickas, *J. High Energy Phys.* **0410** (2004) 066.

[15] S. Profumo, *Phys. Rev. D* **68** (2003) 015006

[16] J. Ellis, K. Olive and Y. Santoso, *Phys. Lett. B* **539** (2002) 107; J. Ellis, T. Falk, K. Olive and Y. Santoso, *Nucl. Phys. B* **652** (2003) 259.

[17] M. Drees, [hep-ph/0410113](#).

[18] A. Brignole, L. E. Ibanez and C. Munoz, *Nucl. Phys. B* **422** (1994) 125 [Erratum-ibid. B **436** (1995) 747]; A. Brignole, L. E. Ibanez, C. Munoz and C. Scheich, *Z. Physik C* **74** (1997) 157.

[19] C. H. Chen, M. Drees and J. Gunion, *Phys. Rev. D* **55** (1997) 330, Erratum-ibid. D **60** (1999) 039901.

[20] R. Dermisek and A. Mafi, *Phys. Rev. D* **65** (2002) 055002; H. Baer, C. Balazs, A. Belyaev, R. Dermisek, A. Mafi and A. Mustafayev, *J. High Energy Phys.* **0205** (2002) 061; C. Balazs and R. Dermisek, *J. High Energy Phys.* **0306** (2003) 024.

[21] H. Baer, M. Diaz, P. Quintana and X. Tata, *J. High Energy Phys.* **0004** (2000) 016.

[22] H. Baer, A. Mustafayev, E. Park and S. Profumo, *J. High Energy Phys.* **0507** (2005) 046.

[23] H. Baer, T. Krupovnickas, A. Mustafayev, E. Park, S. Profumo and X. Tata, *J. High Energy Phys.* **0512** (2005) 011.

[24] N. Arkani-Hamed, A. Delgado and G. F. Giudice, [hep-ph/0601041](#) (2006).

[25] G. Belanger, F. Boudjema, A. Cottrant, A. Pukhov and A. Semenov, *Nucl. Phys. B* **706** (2005) 411.

[26] Y. Mambrini and E. Nezri, [hep-ph/0507263](#) (2005).

[27] H. Baer and X. Tata, *Weak Scale Supersymmetry: From Superfields to Scattering Events*, (Cambridge University Press, 2006).

- [28] L. E. Ibanez and G. G. Ross, *Phys. Lett.* **B 110** (1982) 215; L. Ibanez, *Phys. Lett.* **B 118** (1982) 73; J. Ellis, D. V. Nanopoulos and K. Tamvakis, *Phys. Lett.* **B 121** (1983) 123; L. Alvarez-Gaume, J. Polchinski and M. B. Wise, *Nucl. Phys.* **B 221** (1983) 495.
- [29] K. Griest and L. Roszkowski, *Phys. Rev.* **D 46** (1992) 3309.
- [30] T. Moroi and L. Randall, *Nucl. Phys.* **B 570** (2000) 455.
- [31] A. Corsetti and P. Nath, *Phys. Rev.* **D 64** (2001) 125010.
- [32] A. Birkedal-Hansen and B. Nelson, *Phys. Rev.* **D 64** (2001) 015008 and *Phys. Rev.* **D 67** (2003) 095006.
- [33] V. Bertin, E. Nezri and J. Orloff, *J. High Energy Phys.* **0302** (2003) 046.
- [34] A. Bottino, F. Donato, N. Fornengo and S. Scopel, *Phys. Rev.* **D 70** (2004) 015005.
- [35] D. Cerdeno and C. Munoz, *J. High Energy Phys.* **0410** (2004) 015; Y. Mambrini and C. Munoz, *JCAP* **0410** (2004) 003 and [hep-ph/0507263](#); see also S. Baek, D. Cerdeno, Y. G. Kim, P. Ko and C. Munoz, [hep-ph/0505019](#).
- [36] A. Masiero, S. Profumo and P. Ullio, *Nucl. Phys.* **B 712** (2005) 86.
- [37] D. N. Spergel *et al.* (WMAP Collaboration), [astro-ph/0603449](#) (2006).
- [38] ISAJET v7.73, by H. Baer, F. Paige, S. Protopopescu and X. Tata, [hep-ph/0312045](#); see also H. Baer, J. Ferrandis, S. Kraml and W. Porod, *Phys. Rev.* **D 73** (2006) 015010.
- [39] IsaRED, by H. Baer, C. Balazs and A. Belyaev, *J. High Energy Phys.* **0203** (2002) 042.
- [40] For a review, see *e.g.* G. Eigen, R. Gaitskell, G. Kribs and K. Matchev, [hep-ph/0112312](#); see also D. Hooper and L. T. Wang, *Phys. Rev.* **D 69** (2004) 035001; W. de Boer, M. Herold, C. Sander and V. Zhukov, [hep-ph/0309029](#).
- [41] P. Gondolo, J. Edsjo, P. Ullio, L. Bergstrom, M. Schelke and E. A. Baltz, [astro-ph/0211238](#).
- [42] J.F. Navarro *et al.*, *Mon. Not. Roy. Astron. Soc.* **349** (2004) 1039, [astro-ph/0311231](#); the adiabatic contraction of the halo follows Blumenthal *et al.*, *Astrophys. J.* **301** (1986) 27. For the halo parameter choices see also Ref. [45].
- [43] H. Baer and J. O’Farrill, *JCAP* **03**, 012 (2004).
- [44] H. Baer, A. Belyaev, T. Krupovnickas and J. O’Farrill, *JCAP* **0404** (2004) 005.
- [45] S. Profumo and P. Ullio, *JCAP* **0407** (2004) 006.
- [46] For a recent analysis, see H. Baer, C. Balazs, A. Belyaev and J. O’Farrill, *JCAP* **0309**, 2003 (007); a subset of earlier work includes M. Goodman and E. Witten, *Phys. Rev.* **D 31** (1985) 3059; K. Griest, *Phys. Rev. Lett.* **61** (1988) 666 and *Phys. Rev.* **D 38** (1988) 2357 [Erratum-ibid. *D 39*, 3802 (1989)]; M. Drees and M. Nojiri, *Phys. Rev.* **D 47** (1993) 4226 and *Phys. Rev.* **D 48** (1993) 3483; V. A. Bednyakov, H. V. Klapdor-Kleingrothaus and S. Kovalenko, *Phys. Rev.* **D 50** (1994) 7128; P. Nath and R. Arnowitt, *Phys. Rev. Lett.* **74** (1995) 4592; L. Bergstrom and P. Gondolo, *Astropart. Phys.* **5** (1996) 263; H. Baer and M. Brhlik, *Phys. Rev.* **D 57** (1998) 567; J. Ellis, A. Ferstl and K. Olive, *Phys. Lett.* **B 481** (2000) 304 and *Phys. Rev.* **D 63** (2001) 065016; E. Accomando, R. Arnowitt, B. Dutta and Y. Santoso, *Nucl. Phys.* **B 585** (2000) 124; A. Bottino, F. Donato, N. Fornengo and S. Scopel, *Phys. Rev.* **D 63** (2001) 125003; M. E. Gomez and J. D. Vergados, *Phys. Lett.* **B 512** (2001) 252; A. B. Lahanas, D. V. Nanopoulos and V. C. Spanos, *Phys. Lett.* **B 518** (2001) 94;

A. Corsetti and P. Nath, *Phys. Rev.* **D 64** (2001) 115009; E. A. Baltz and P. Gondolo, *Phys. Rev. Lett.* **86** (2001) 5004; M. Drees, Y. G. Kim, T. Kobayashi and M. M. Nojiri, *Phys. Rev.* **D 63** (2001) 115009; see also J. Feng, K. Matchev and F. Wilczek, *Phys. Lett.* **B 482** (2000) 388 and *Phys. Rev.* **D 63** (2001) 045024; R. Ellis, A. Ferstl, K. A. Olive and Y. Santoso, *Phys. Rev.* **D 67** (2003) 123502; J. R. Ellis, K. A. Olive, Y. Santoso and V. C. Spanos, *Phys. Rev.* **D 69** (2004) 015005; see C. Munoz, [hep-ph/0309346](#) for a recent review.

- [47] See H. Baer, C. Balazs, A. Belyaev and J. O'Farrill, Ref. [46]
- [48] D. S. Akerib *et al.* (CDMS Collaboration), [astro-ph/0405033](#) (2004).
- [49] A. Benoit *et al.* (Edelweiss Collaboration), *Phys. Lett.* **B 545** (2002) 43.
- [50] M. Bravin *et al.* (CRESST Collaboration), *Astrophys. J.* **12** (1999) 107.
- [51] N. Spooner *et al.* (Zeplin-1Collaboration), in *Proc. of the APS/DPF/DPB Summer Study on the Future of Particle Physics (Snowmass 2001)* ed. N. Graf, eConf **C010630**, E601 (2001).
- [52] Y. Suzuki *et al.* (Xenon Colaboration), [hep-ph/0008296](#).
- [53] I. Abt *et al.*, [hep-ex/0404039](#).
- [54] D. B. Cline *et al.* (ZEPLIN-4 Collaboration), *Nucl. Phys.* **124** (*Proc. Suppl.*) (2003) 229.
- [55] See talk by C. Rubbia at 6th UCLA Symposium on *Sources and Detection of Dark Matter and Dark Energy in the Universe*, Marina del Ray, CA, February (2004).
- [56] J. Silk, K. Olive and M. Srednicki, *Phys. Rev. Lett.* **55** (1985) 257; K. Freese, *Phys. Lett.* **B 167** (1986) 295; L. Krauss, M. Srednicki and F. Wilczek, *Phys. Rev.* **D 33** (1986) 2079; V. Berezinsky, A. Bottino, J. R. Ellis, N. Fornengo, G. Mignola and S. Scopel, *Astropart. Phys.* **5** (1996) 333; L. Bergstrom, J. Edsjo and P. Gondolo, *Phys. Rev.* **D 55** (1997) 1765 and *Phys. Rev.* **D 58** (1998) 103519; A. Bottino, F. Donato, N. Fornengo and S. Scopel, *Astropart. Phys.* **10** (1999) 203; A. Corsetti and P. Nath, *Int. J. Mod. Phys.* **A 15** (2000) 905; V. Barger, F. Halzen, D. Hooper and C. Kao, *Phys. Rev.* **D 65** (2002) 075022; V. Bertin, E. Nezri and J. Orloff, *Eur. Phys. J.* **C 26** (2002) 111 and *J. High Energy Phys.* **0302** (2003) 046.
- [57] E. Carmona *et al.*, (Antares Collaboration), *Nucl. Phys.* **95** (*Proc. Suppl.*) (2001) 161.
- [58] J. Ahrens *et al.*, (IceCube Collaboration), *Nucl. Phys.* **118** (*Proc. Suppl.*) (2003) 388; F. Halzen, [astro-ph/0311004](#); F. Halzen and D. Hooper, *JCAP* **0401** (2004) 002.
- [59] F. Stecker, *Phys. Lett.* **B 201** (1988) 529; F. W. Stecker and A. J. Tylka, *Astrophys. J.* **343** (1989) 169; S. Rudaz and F. Stecker, *Astrophys. J.* **368** (1991) 406; M. Urban *et al.*, *Phys. Lett.* **B 293** (1992) 149; V. Berezinsky, A. Gurevich and K. Zybin, *Phys. Lett.* **B 294** (1992) 221; V. Berezinsky, A. Bottino and G. Mignola, *Phys. Lett.* **B 325** (1994) 136; L. Bergstrom, P. Ullio and J. H. Buckley, *Astropart. Phys.* **9** (1998) 137; L. Bergstrom, J. Edsjo and P. Ullio, *Phys. Rev.* **D 58** (1998) 083507; J. Buckley *et al.*, [astro-ph/0201160](#); P. Ullio, L. Bergstrom, J. Edsjo and C. Lacey, *Phys. Rev.* **D 66** (2002) 123502.
- [60] H. A. Mayer-Hasselwander *et al.* (EGRET Collaboration), MPE-440 (1998).
- [61] A. Morselli *et al.*, (GLAST Collaboration), *Nucl. Phys.* **113** (*Proc. Suppl.*) (2002) 213.
- [62] S. Rudaz and F. Stecker, *Astrophys. J.* **325** (1988) 16; A. Tylka, *Phys. Rev. Lett.* **63** (1989) 840; M. Turner and F. Wilczek, *Phys. Rev.* **D 42** (1990) 1001; M. Kamionkowski and M. Turner, *Phys. Rev.* **D 43** (1991) 1774; A. Moskalenko and A. Strong, *Phys. Rev.* **D 60** (1999)

063003; E. Baltz and J. Eds  , *Phys. Rev. D* **59** (1999) 023511; G. Kane, L. T. Wang and J. Wells, *Phys. Rev. D* **65** (2002) 057701; E. Baltz, J. Eds  , K. Freese and P. Gondolo, *Phys. Rev. D* **65** (2002) 063511; G. Kane, L. T. Wang and T. Wang, *Phys. Lett. B* **536** (2002) 263; D. Hooper, J. Taylor and J. Silk, [hep-ph/0312076](#).

[63] M. A. DuVernois *et al.* (HEAT Collaboration), *Astrophys. J.* **559** (2001) 296.

[64] M. Pearce (Pamela Collaboration), *Nucl. Phys. 113 (Proc. Suppl.)* (2002) 314.

[65] J. Casaus *et al.* (AMS Collaboration), *Nucl. Phys. 114 (Proc. Suppl.)* (2003) 259.

[66] F. Stecker, S. Rudaz and T. Walsh, *Phys. Rev. Lett.* **55** (1985) 2622; F. Stecker and A. J. Tylka, *Astrophys. J.* **336** (1989) L51; P. Chardonnet, Mignola, P. Salati and R. Taillet, *Phys. Lett. B* **384** (1996) 161; A. Bottino, F. Donato, N. Fornengo and P. Salati, *Phys. Rev. D* **58** (1998) 123503; L. Bergstrom, J. Eds   and P. Ullio, *Astrophys. J.* **526** (1999) 215.

[67] S. Orito *et al.* (BESS Collaboration), *Phys. Rev. Lett.* **84** (2000) 1078.

[68] H. Fuke *et al.* (BESS Collaboration), [astro-ph/0504361](#).

[69] K. Mori, C. J. Hailey, E. A. Baltz, W. W. Craig, M. Kamionkowski, W. T. Serber and P. Ullio, *Astrophys. J.* **566** (2002) 604, C. J. Hailey *et al.*, *JCAP* **0601** (2006) 007 [[arXiv:astro-ph/0509587](#)].

[70] S. Profumo and C.E. Yaguna, *Phys. Rev. D* **70** (2004) 095004

[71] H. Baer and S. Profumo, *JCAP* **0512** (2005) 008.

[72] A. W. Strong and I. V. Moskalenko, [arXiv:astro-ph/0106504](#).

[73] P. Picozza and A. Morselli, *J. Phys. G* **29** (2003) 903 [[arXiv:astro-ph/0211286](#)].

[74] H. Baer and E. Berger, *Phys. Rev. D* **34** (1986) 1361; H. Baer, X. Tata and J. Woodside, *Phys. Rev. Lett.* **63** (1989) 352, *Phys. Rev. D* **41** (1990) 906 and *Phys. Rev. D* **44** (1991) 207; H. Baer, C. Kao and X. Tata, *Phys. Rev. D* **48** (R2978) 1993; H. Baer, C. H. Chen, C. Kao and X. Tata, *Phys. Rev. D* **52** (1995) 1565; H. Baer, C. H. Chen, F. Paige and X. Tata, *Phys. Rev. D* **54** (1996) 5866; H. Baer, C. H. Chen, M. Drees, F. Paige and X. Tata, *Phys. Rev. D* **58** (1998) 075008. For an overview, see S. Abel *et al.*, Report of the mSUGRA working group for the workshop on Physics at Run II at the Tevatron, [hep-ph/0003154](#).

[75] See *e.g.* H. Baer, X. Tata and J. Woodside, *Phys. Rev. D* **42** (1990) 1568.

[76] H. Baer, K. Hagiwara and X. Tata, *Phys. Rev. D* **35** (1987) 1598; H. Baer, D. Dzalo-Karatas and X. Tata, *Phys. Rev. D* **42** (1990) 2259; H. Baer, C. Kao and X. Tata, *Phys. Rev. D* **48** (1993) 5175; H. Baer, C. H. Chen, F. Paige and X. Tata, *Phys. Rev. D* **50** (1994) 4508. I. Hinchliffe *et al.*, *Phys. Rev. D* **55** (1997) 5520 and *Phys. Rev. D* **60** (1999) 095002; H. Bachacou, I. Hinchliffe and F. Paige, *Phys. Rev. D* **62** (2000) 015009; Atlas Collaboration, LHCC 99-14/15; C. Lester, M. Parker and M. White, *J. High Energy Phys.* **0601** (2006) 080.

[77] H. Baer, J. Ellis, G. Gelmini, D. V. Nanopoulos and X. Tata, *Phys. Lett. B* **161** (1985) 175; G. Gamberini, *Z. Physik C* **30** (1986) 605; H. Baer, V. Barger, D. Karatas and X. Tata, *Phys. Rev. D* **36** (1987) 96; H. Baer, X. Tata and J. Woodside, *Phys. Rev. D* **45** (1992) 142.

[78] R. M. Barnett, J. Gunion and H. Haber, *Phys. Lett. B* **315** (1993) 349; H. Baer, X. Tata and J. Woodside, Ref. [74].

- [79] H. Baer, C. H. Chen, F. Paige and X. Tata, *Phys. Rev.* **D 52** (1995) 2746 and *Phys. Rev.* **D 53** (1996) 6241; H. Baer, C. H. Chen, M. Drees, F. Paige and X. Tata, *Phys. Rev.* **D 59** (1999) 055014; S. Abdullin and F. Charles, *Nucl. Phys.* **B 547** (1999) 60; S. Abdullin *et al.* (CMS Collaboration), [hep-ph/9806366](#); B. Allanach, J. Hetherington, A. Parker and B. Webber, *J. High Energy Phys.* **08** (2000) 017.
- [80] H. Baer, C. Balazs, A. Belyaev, T. Krupovnickas and X. Tata, *J. High Energy Phys.* **0306** (2003) 054.
- [81] P. G. Mercadante, J. K. Mizukoshi and X. Tata, *Phys. Rev.* **D 72** (2005) 035009.
- [82] I. Hinchliffe *et al.*, Ref. [76]; H. Bachacou, I. Hinchliffe and F. Paige, Ref. [76]; Atlas Collaboration, LHCC 99-14/15.
- [83] H. Baer, A. Belyaev, T. Krupovnickas and X. Tata, *J. High Energy Phys.* **0402** (2004) 007; H. Baer, T. Krupovnickas and X. Tata, *J. High Energy Phys.* **0406** (2004) 061; see also H. Baer, R. Munroe and X. Tata, *Phys. Rev.* **D 54** (1996) 6735.
- [84] S. Y. Choi *et al.*, *Eur. Phys. J.* **C14** (2000) 535.
- [85] H. Baer *et al.*, in preparation.